SYNTHESIS, CHARACTERIZATION AND PHYSICOCHEMICAL PROPERTIES OF PLATINUM NANOPARTICLES ON ORDERED MESOPOROUS CARBON

Waheed Saban

B. Sc (Hons) Chemistry

M.Sc thesis submitted in fulfilment of the requirements for the degree of Magister Scientiae,

In the Department of Chemistry, Environmental and Nanosciences Group,

University of Western Cape

Supervised By: Prof. L. F. Petrik

Co–supervised By: Dr S Titinchi

May 2011

DECLARATION

"I declare that the SYNTHESIS, CHARACTERIZATION AND PHYSIOCHEMICAL PROPERTIES OF PLATINUM NANOPARTICLES ON ORDERED MESOPOROUS CARBON, is my own work, that it has not been submitted for any degree or examination in any other University and that all sources I have used or quoted have been indicated and acknowledged by complete references."

Name:_____

Signed:_____

Date:_____

ACKNOWLEDGEMENTS

I would like to express my profound and my deepest gratitude to the Almighty for bestowing on me the gift of life and opportunities in order that I may serve him to the best of my ability.

My parents, for their upbringing and constant motivation have allowed me to fulfill my ambition.

Prof Leslie Petrik and Dr Salam Titinchi for their guidance and tutelage and immense scientific contributions.

I would also like to acknowledge Dr Patrick Ndungu for his scientific contributions.

I would like to thank Dr Hanna Abbo for assisting me with the electrochemical characterization of my nanophase electrocatalyst.

Dr Remy Butcher for assisting me with XRD analysis.

The University of Western Cape, Department of Physics for their assistance with SEM and HRTEM characterization.

Colleagues and fellow graduates and the staff of the Environmental and Nanosciences Group at UWC for their support and making my laboratory work a much more interesting place.

And lastly, I would like to thank my wife for always showing her unconditional love and support for me during my studies.

KEYWORDS

Nanoparticles

Electrocatalysts

Porous Materials

Silica substrates

Mesoporous support

Carbons

Chemical Vapour Deposition

Platinum

Fuel cells

Hydrogen Production

ABSTRACT

Nanoarchitecture of platinum group metals (PGM's) and the design of pure and alloy metal catalyst is an area of intense R & D, especially for the hydrogen energy technologies. But just as important as the PGM nanoparticles, is the rational design of the support material, and the understanding of how this affects the PGM nanoparticles in specific applications. This research is aimed at improving the design, fabrication and performance of nanophase electrocatalyst, both nanoparticles and the supports, and understanding how to engineer supports for novel functional composite nanophase PGM metal catalyst for specific applications in energy related applications. The other objective of this study was to evaluate the synthesized catalysts (supported Pt metal on ordered mesoporous carbon) and understand the role of the carbon support for the application in fuel cells.

In this study SBA-15 mesoporous silica template was synthesized and used as a sacrificial template in the preparation of ordered mesoporous carbon material. A chemical vapour deposition (CVD) technique using LPG or alternatively sucrose, pyrolyzed upon a mesoporous Si matrix were used to produce nanostructured ordered mesoporous carbon (OMC) with graphitic character after removing the Si template. The sucrose method was found to be a suitable route for preparing OMC. The OMC was used as a conductive three dimensional porous support for depositing catalytic nanophase Pt metal. Deposition of Pt nanoparticles on OMC was accomplished using a CVD method with $Pt(acac)_2$ as a precursor. The synthesized nano-composite materials were characterized by several techniques such as, HRTEM, HRSEM, EDS, XRD, BET, TGA, FT-IR and CV.

Pt electrocatalyst supported on OMC was synthesized effectively. The results showed that Pt particle sizes of the prepared Pt/OMC catalysts were between 2 and 3 nm for the 20% Pt/OMC catalyst. The electrochemically active surface area study of Pt/OMC and the commercial Johnson Matthey (JM) catalyst were both determined in H_2SO_4 using cyclic voltammetry.

The Pt/OMC showed promising results during chemically active surface area investigation, which compared well with a commercial standard JM Pt/C catalyst.

The most significant result attained in this study was the preparation of a high surface area OMC support using SBA-15 silica template and sucrose as a source of carbon. In addition, a high loading and uniform distribution of Pt nanoparticles on the OMC using a simplified CVD method was successfully achieved.

ABBREVIATIONS

BET	Brunauer-Emmett-Teller
BJH	Barret-Joyner-Halenda
CMS	Carbon microspheres
CV	Cyclic voltammetry
CVD	Chemical vapour deposition
DMFC	Direct methanol fuel cell
EAS	electrochemical active surface
EDS	Energy dispersive spectroscopy
FTIR	Fourier transform infrared
H_2SO_4	Sulphuric acid
HMS	Hexagonal Mesoporous Silica
HRSEM	High resolution scanning electron microscopy
HRTEM	High resolution electron microscopy
HSAG	High surface area graphite
I	Current density
JM	Johnson matthey™
LPG	Liquid petroleum gas
MCM	Mobile company of matter
MCN	Mesoporous carbon nanopartcles
MPAC	Mesoporous active carbon
MSM	Mesostructured silica materials
OMC	Ordered mesoporous carbon
OMCVD	Organometallic chemical vapour deposition
ORR	Oxygen reduction reaction
PEM	Proton exchange membrane
PEMFC	Proton exchange membrane fuel cell
PGM's	Platinum group metals
PSD	Pore size distribution
R&D	Research and development

SBA	Santa barbara amorphous
SEM	Scanning electron microscopy
TEOS	Tetraethoxysilane
TGA	Thermo – gravimetric analysis
V	Voltage
XRD	X – ray diffraction
θ	Theta angle
λ	Wavelength

TABLE OF CONTENTS

List of Tables

List of Figures

List of Schemes

CHAPTER 1

1. INTRODUCTION AND OVERVIEW

The science of nanotechnology was pioneered by Norio Taniguchi (1974), and aimed to elucidate the atomic world that measures matter in nanometers. The area of nanoscience has garnered great attention because of the development of new materials by the assembly of small particles referred to as nanoparticles. Nanoparticles can be described as being approximately 0.1 – 100 nm in size. Such particles exhibit interesting features at these magnitudes and smaller, as they present different properties from the bulk material. These nanoparticles can be manipulated and transformed to improve the technology of manufacturing, microelectronics, computation, and medicine (Horenstein, 2009).

There has been growing interest in the use of nanocarbons as supports for direct methanol fuel cell (DMFC) catalysts to achieve excellent electrocatalytic behavior and also to make use of the structural properties that these material exhibit. Ordered Mesoporous Carbon (OMC) material has been used as a support material for improving the performance of DMFCs because of their large surface area and mesoporous structure (Chang *et al.*, 2007). This study addresses the development of nanostructured support materials for dispersing and stabilizing nanoparticulate platinum electrocatalysts. It is believed that South Africa is set to gain from the diversification of Pt containing materials and their application in the emerging hydrogen economy.

This chapter introduces the dissertation topic and identifies the main perspective as initiated by the problem statement and the rationale and motivation. The main research questions are identified and the research framework and the research approach are presented.

1.1 DISSERTATION TOPIC AND MAIN PERSPECTIVE

The aim of this research was to gain a fundamental understanding of the design, fabrication and performance of nanophase structures in order to obtain carbon supported nanophase Pt catalysts. The fabrication of nanostructured PGMs was developed, measured, described, compared and evaluated for their catalytic behaviour. A further objective is to show that the structure of catalysts in the mesoporous environment can produce a significant impact on metal (Pt) dispersion, reducibility and catalytic performance in this material.

The purpose of this research was to enhance the surface area of platinum group metals (PGMs) supported on nanophase carbon material; such materials may be applied as electrocatalysts in electrode systems for fuel cell applications. The type of carbon material which supports the catalyst may influence the dispersion and size of the metal clusters. The synthesis of nanophase Pt based catalysts with high surface area has gained significant interest for the development of catalyst, fuel cells and chemical sensors. These catalysts are also excellent materials for the oxidation of small organic molecules (SOM) (Wang *et al.,* 2009).

The structural parameters of ordered mesoporous carbons, such as pore structure, pore size, particle morphology, and surface area, is very important for developing a fuel cell support. The improvement of the area of electrode / electrolyte interface will enhance the charge transport of a Pt catalyst. The porous support materials with suitable pore structure, large surface area provides a good way to increase the interfacial area as well as decrease the electrolyte ion diffusion distance (Kong *et al.,* 2010).

Various nanostructured carbons such as nanotubes, nanofibers, nanocoils and ordered mesoporous carbons (OMCs) all show characteristics as substrates for metal stabilization in fuel cells applications (Ambrosio *et al.,* 2008).. OMC will be investigated in this study because of its high specific surface area, its good conductivity (related to the degree of graphitization), its high number of ordered mesopores and its low production cost. OMCs can be achieved as the inverse replica of ordered mesoporous silica templates (Ambrosio *et al.,* 2008).

In this study a nanophase Pt based electrocatalyst was supported on mesoporous Si and carbon supports. This was achieved by impregnating a Pt salt containing solution upon a high surface area hexagonal mesoporous silica matrix, which was then carbonized to varying degrees by chemical vapour deposition of LPG. It was shown that Pt nanophases were stabilized and well dispersed on both the parent Hexaganol Mesoporous Silica (HMS) and the OMC analogue based on the HMS mesoporous supports, without agglomeration (Petrik *et al.,* 2008).

1.2 RATIONALE AND MOTIVATION

The main reason for undertaking this research is to evaluate the effectiveness of nanosized platinum that could replace the bulk form of Pt. Gasteiger *et al.* (2005) reports that the reduction in platinum content can be effected in two ways: (i) improvement of the catalyst activity and efficiency, either by optimizing the metal dispersion or by using appropriate alloys and (ii) improvement of the electrode structure in order to decrease the diffusion-induced potential losses.

The catalytic activity of PGMs depends largely on metal particle size and surface area which plays a crucial role in oxygen reduction kinetics for fuel cells. The incorporation of transition metals into this catalyst increases the catalytic activity and reduces the cost (i) the Pt – based alloys show higher activity than Pt alone (Li *et al.,* 2004).

This research will identify the conditions under which a mesoporous carbon support can be prepared so that a highly dispersed Pt can be supported on it in order that the highest surface area with the greatest electrocatalytic activity is achieved. This research involves the use of mesoporous silica materials such as SBA-15 as sacrificial templates for the preparation of OMC. The findings of the proposed research would contribute to the successful design of supported PGMs as catalysts.

1.3 PROBLEM STATEMENT

It is well known that a high surface area OMC can be successfully synthesized using SBA-15 as a sacrificial template with defined pore sizes. Previous studies (Petrik *et al.,* 2008) have demonstrated that preparing and producing a high surface area ordered

mesoporous carbon support material is problematic. Problems may arise from a number of variables such as temperature, rate of heating and other conditions in which the carbonization process takes place. The variables used during the initial synthesis process were not adequately optimized and it was found that the pore walls of the silica mesoporous materials used were not stable. The issue requiring investigation was to establish which Si matrix and carbonization method could produce the highest stability and highest surface area ordered mesoporous carbon. Thereafter the degree of Pt dispersion in terms of agglomeration and sintering of the catalyst on the ordered mesoporous carbon supports could be evaluated.

1.4 RESEARCH APPROACH

In this work a chemical vapour deposition and another carbon deposition procedure were used for the synthesis of a mesoporous carbon material. SBA-15 silica template was used as a sacrificial template to obtain a high surface area mesoporous carbon. In the first instance, SBA-15 template was utilised for the preparation of a carbon analogue using the non–catalytic chemical vapour deposition pyrolysis (CVD) of liquid petroleum gas (LPG) as a carbon precursor. The LPG was used to infiltrate the pores of SBA-15. A more conventional procedure was investigated making use of sucrose for the preparation of the carbon analogues. These methods both involved the initial impregnation of the Si templates with the carbon source, subsequent carbonisation of the impregnated template, followed by dissolution of the silica framework with NaOH through chemical etching to produce a high surface mesoporous carbon analogue. Platinum nanoparticles were deposited onto the OMC using a CVD method. This involved the use of $Pt(acac)_2$ and depositing Pt nanoparticles onto OMC under high temperature and pressure using a CVD method.

1.5 SCOPE OF STUDY

This thesis examined the use of SBA-15 as template materials that were employed as a sacrificial template for the synthesis of Ordered Mesoporous Carbon (OMC) using LPG during Carbon Vapour Deposition (CVD) and an impregnation method using sucrose as a

carbon sources to achieve the desired OMC. Thereafter, the dispersion of Pt nanoparticles on these OMC materials was investigated and the resulting electrocatalysts were characterised and compared to an industry standard. The electrocatalytic activity of Pt/OMC was compared against a commercial industry standard using cyclic voltammetry.

1.6 DELIMITATIONS OF THE STUDY

- SBA-15 was the silica substrate that was used as a sacrificial template.
- SBA-15 possesses a thick pore wall and the hydrothermal stability is much higher than the corresponding MCM-41 and HMS supports. This template was preferred above HMS and MCM-41 in this study.
- Carbonization was only investigated using either the CVD with LPG source or infiltration method with sucrose.
- The only chemical etchant of the Si matrix that was investigated in this study was NaOH and not other etchants such as HF.

1.7 RESEARCH QUESTIONS

- Which carbonization method is the most successful in achieving a high surface area mesoporous carbon support for nanoparticulate platinum dispersion?
- Can SBA-15 matrix be used as a sacrificial template to produce a high surface area OMC?
- What are the surface area, pore volume and pore diameters of the SBA-15?
- What are the surface area, pore volume and pore diameters of the OMC?
- Can Pt be dispersed upon the carbon substrate and be stabilized?
- How do the synthesised materials compare to a commercial standard in electrocatalytic activity?
- Are the materials suitable electrocatalysts for hydrogen production?

1.8 RESEARCH HYPOTHESIS

The research hypothesis was that; i) a high surface area mesoporous carbon may be achieved by use of a silica template with high surface area by employing LPG or sucrose

as carbon sources. (ii) Platinum nanoparticles can be deposited with high dispersion into the pores of the mesoporous carbon using a chemical vapour deposition method.

1.9 STRUCTURE OF THESIS

The thesis will be presented according to the following outline:

Chapter 1: This chapter covers the introduction and overview of the dissertation topic.

Chapter 2: This chapter covers the literature on the different mesoporous silica materials that can be used to achieve a high surface area mesoporous carbon support. This chapter also includes the synthesis, characterisation, catalytic and technical applications of mesoporous carbon materials as well as electrocatalytic performance of Pt.

Chapter 3: This chapter covers the experimental methods and materials used in this study. The details of preparation and characterisation of the ordered carbon support material is outlined. Mesoporous silica materials were used as support or as sacrificial template for the preparation of carbon analogues. LPG and sucrose were used as carbon sources for the deposition of carbon into the pore volume of such sacrificial matrixes which was followed by pyrolysis of the carbonaceous materials and finally removal of the silica matrix resulting in an ordered mesoporous carbon (OMC) analogue. Characterisation was done using Fourier Transform Infra – red (FTIR) Spectroscopy, High Resolution Electron Microscopy (HRTEM)/ Energy Dispersive Spectroscopy (EDS), Scanning Electron Microscopy (SEM)/ Energy Dispersive Spectroscopy (EDS), X–Ray Diffraction (XRD), Brunnaer – Emmet – Teller (BET) surface area analysis, Thermal Gravimetric Analysis (TGA) and electrochemical characterization of the consolidated composite material using cyclic voltammetry (CV).

Chapter 4: This chapter covers the results and discussion illustrating the synthesis of carbon materials. It first starts with the synthesis of the amorphous silica material and then the impregnation of the silica mesostructure with a

suitable carbon source such as sucrose and finally the decomposition of the silica material to obtain the desired mesoporous carbon. The deposition of platinum takes place directly onto the surface of the mesoporous carbons materials via chemical vapour deposition. The characterisation of the mesoporous silica and carbon supported material as well as the electrochemical results of the PtOMC material are outlined in this chapter.

Chapter 5: Finally, in chapter 5, the overall conclusions are presented and recommendations for future studies are made. The last chapter is followed by a complete list of references.

CHAPTER 2

LITERATURE REVIEW

2. PLATINUM NANOPARTICLES ON AN ORDERED MESOPOROUS CARBON SUPPORT

This literature review outlines the general principles used in the synthesis of nanophase silica and carbon materials as well as the physico-chemical and electrocatalytic properties of these nanomaterials. The characterisation of these nanophases is briefly discussed and the properties influencing the behaviour of nanophase electrocatalysts is identified. It was necessary to introduce the problem areas, applications and the properties of these nanophase materials as briefly discussed in Chapter 1.

2.1 BOUNDARIES OF THE LITERATURE REVIEW

This literature review will describe the term "porous materials" and describe the physico-chemical properties of these materials, upon decreasing their particle size from the bulk to the nanometre region. The synthetic approach used for producing nanomaterials and their electrocatalytic behaviour is also outlined. Thereafter, the properties of nanomaterials will be assessed in terms of its suitability as nanophase electrocatalysts.

2.2 KEY CONCEPTS

According to IUPAC, porous material can have three different pore types that are responsible for the porosity of carbon materials; that is, micropores (pore size < 2 nm), mesopores (2 nm < pore size < 50 nm) and macropores (pore size > 50 nm) (Ambrosio *et al.,* 2008).

The design of mesoporous materials for various applications has huge potential for the development of novel solid catalyst because of their high surface area, and narrow and uniform pore size distribution (Taguchi *et al.,* 2005).

Various types of mesoporous materials have been synthesized or studied such as Hexagonal Mesoporous Silica (HMS), Mobil Company of Matter (MCM–41) and MCM–48, Santa Barbara Amorphous (SBA–15), etc.(Vinu *et al.,* 2006; Gaydhankar *et al.,* 2006; Vartuli, *et al.,* 1994; Setoguchi *et al.,* 1997; Orge *et al.,* 2009).

Ordered mesoporous carbon (OMC) has generated significant interest due to its high surface area, uniform pore diameters, large adsorption capacities, high thermal, acid-base, and mechanical stabilities (Kong *et al.,* 2010; Lin *et al.,* 2005).

Ryoo *et al.,* (1999) reported the synthesis of porous carbons with a large surface area, a high porosity and controlled narrow pore size distributions (PSDs) using mesostructured silica materials as templates.

Carbon microspheres (CMS) have potential applications in the development of a support for metal catalysts. The activity of the CMS-supported catalysts is dependant on the percentage of catalyst loading. The CMS-supported catalysts illustrated significant stable activity on stream for a long duration of time. The preparation of pure carbon spheres was attained in the absence of a catalyst through the direct pyrolysis of two hydrocarbon sources, acetylene and ethylene (Mhlanga *et al.,* 2009).

The efficiency of a Pt-based fuel cell catalyst is determined by the size and distribution of metal particles; and good dispersion of the catalyst particles for the oxygen reduction reaction (ORR) to improve the electrode kinetics (Ambrosio *et al.,* 2009).

Cyclic voltammetry (CV) has been applied to examine the surface area (as electrochemical active surface (EAS)) of Pt/C catalysts by adsorption of atomic hydrogen in acidic media (Pozio *et al.,* 2002; Chen *et al.,* 2011).

2.3 SILICA SUBSTRATES

2.3.1 MESPOROUS SILICA MATERIALS

Mesoporous materials have been recently recognized as having widespread use in areas such as catalysis (Vinu *et al.,* 2006), adsorption (Vinu *et al.,* 2006), separation (Vinu *et*

al., 2006), sensing (Vinu *et al.,* 2006), medical usage (Vinu *et al.,* 2006), ecology (Vinu *et al.,* 2006), and nanotechnology (Vinu *et al.,* 2006). They can be classified as porous materials with diameters in the size range of 0.2 – 2 nm. The discovery of the M41S family of materials which have large uniform structures, high specific surface areas and specific pore volumes, including hexagonal MCM–41, cubic MCM–48, and lamellar MCM–50 materials. This family of materials was discovered by Mobil scientists (Kresge, 1992). The preparation of mesoporous materials (such as HMS, MCM–41 and SBA–15) can be achieved forming silica structures around a micelle assemblies followed by template removal as demonstrated in Figure 2.1, (Vinu *et al.,* 2006).

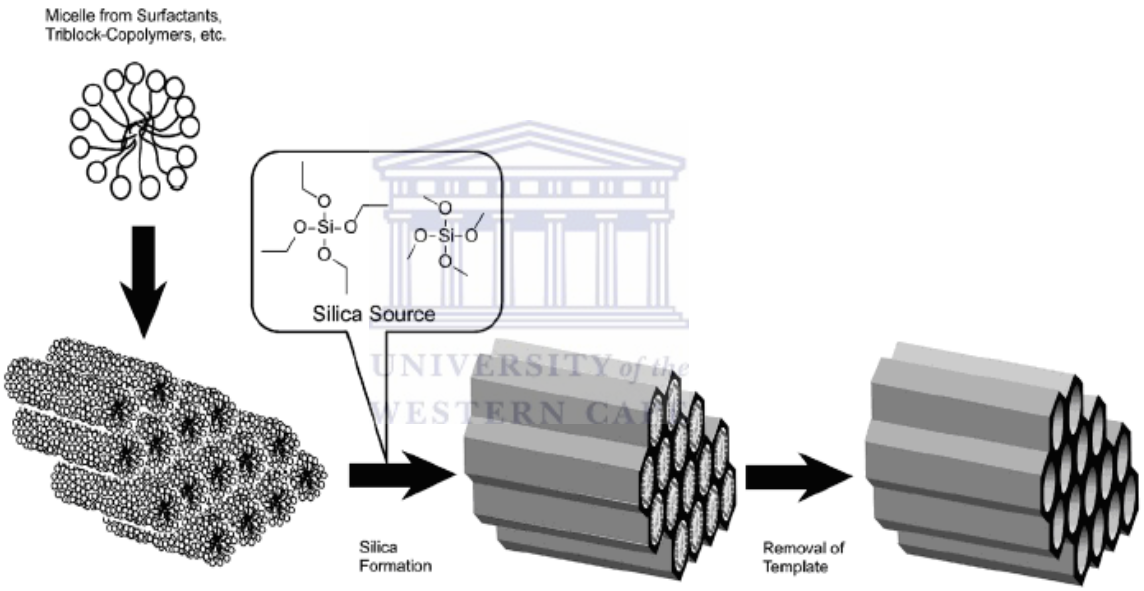

Figure 2.1: General concept for synthesis of mesoporous silica from micelle template. (Vinu *et al.,* 2006)

2.3.2 MESOPOROUS SILICA SPHERES

MCM–41 and MCM–48 are considered the most important members of the M41S micelle templated mesoporous materials. MCM–48 in particular has a body-centred cubic structure with Ia 3d (No 230) space group symmetry and demonstrates a 3D channel system. The structure of these materials has not been fully investigated; however, the walls of the channels are formed from an amorphous hydroxylated silicate.

MCM–41 comprises of a hexagonal or honeycomb packing of uniform mesopore channels. They have pores which are arranged differently from MCM–48 and they

demonstrate a 1D channel system. Thus new syntheses were then developed and optimised by manipulating the g packing parameter. The g packing parameter refers to the effective surfactant ion pair packing parameter, g=V/aα , is mediated in the range of 1/3 - ½ with the increment of V and l, thus indicating that mesoporous silica is a well-ordered hexagonal structure.These materials were structurally characterised by means of X-ray diffraction (XRD) (Van Tendeloo *et al.,* 2003). This technique allows the capturing of information on the long range ordering of the pores. XRD interpretation is hindered by the large unit cell as a result of diffraction peaks in the small-angle region. A broadening of the peaks, induced by the small crystal size, further reduces the accuracy, especially when several phases are present. High-resolution transmission electron microscopy (HRTEM), in combination with electron diffraction (ED), is therefore more effective in ascertaining the structure of mesoporous materials on a local scale (Van Tendeloo *et al.,* 2003).

2.3.3 ORDERED MESOPOROUS SILICA EMPLOYED AS A CATALYST

Ordered mesoporous silica's have been commonly used as a catalyst. The silica can be prepared by the incorporation of active sites into the silica walls or by deposition of the active species on the inner surface of the material. The benefits of using these solid materials in catalysis are; the relatively large pores which assist in mass transfer and the high surface area permitting a high concentration of active species per mass of material. Mesoporous materials can be tailored in many ways to provide novel catalytic functions as represented in Figure 2.2.

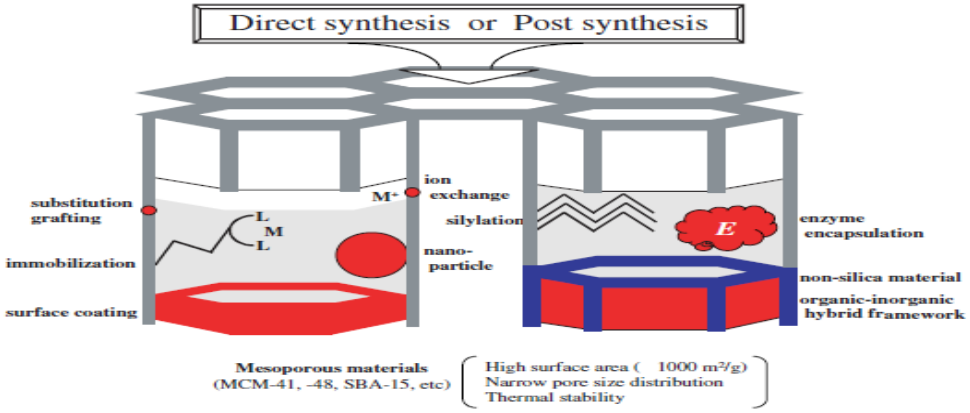

Figure 2.2: Schematic sketch of the various methods for the functionalization of mesoporous material (Taguchi, 2005).

The metal ions replacing the silicon atoms in the support, analogous to zeolites, can be used as acid or redox active sites and may be utilized in diverse ways of catalytic reactions. The wall structure of these ordered mesoporous silica bear a resemblance to amorphous silica, and the incorporation of other metal centres does not give way to definite sites as in zeolites. To a certain extent the material affords a mixture of different sites with diverse local environments (Taguchi, 2005).

The catalytic properties of these materials are relatively nearer to those of metal substituted amorphous silica, than to those of framework substituted zeolites. The more attractive component includes the exceptionally high surface area of these materials for supported metal or metal oxide particles, the ability to deposit isolated species on the wall structure (Taguchi, 2005).

The variations used to prepare these ordered mesoporous materials are quite considerable, and the properties of these materials can be modified individually. The structure of mesoporous materials can be altered by the addition of various constituents. These changes utilize the silanol groups present on the silica surface of the ordered mesoporous silica, since they are the anchor sites for metal species. The density of silanols in ordered mesoporous materials particularly in MCM–41 is lower than in traditional hydroxylated silica. The density of silanol groups is stable in traditional hydoxylated silica, approximately 4 – 6 Si–OH/nm^2, whereas ordered mesoporous materials have displayed different concentrations of between 1.4 and 1.9 group/ nm^2 for MCM–48 (Taguchi, 2005).

2.4 CARBON MATERIALS

2.4.1 INTRODUCTION

It is well known that carbon is found in different forms from diamond gemstones to C_{60} fullerene and graphite to carbon nanotubes. The high surface area forms of carbon are commonly associated with activated and porous charcoals. The latter form is made from wood, peat and coconut husk. This form of carbon has been used as a support to prepare platinum group metal (PGMs) catalyst, that usually consist of a small amount of PGMs displaying high activities at low temperature (Twigg, 2009).

These catalysts have high intrinsic catalytic activity. They can be dispersed over activated charcoals, as extremely small crystallites that provide high surface areas of the active metal. These catalysts, and especially those containing palladium, have been used extensively for many years in organic preparative chemistry. They are still found in carbon–carbon bond forming processes and potentially, also indirect carbonylation reactions (Twigg, 2009).

2.4.1.1 CARBON IN THE ROLE AS A CATALYST

Studies have shown that it is possible to use carbon as a catalyst with the carbon the an active component. This process is carried out by the concurrent action of two principles. The first principle is the selective chemisorption of a reactant at the carbon, through either ion-exchange or directly through the dispersive forces in relation to the graphite valence electronic system. The subsequent principle is the production of atomic oxygen taking place on every carbon material that has a graphene face. These protocols are essential to catalysis, especially surface patches with an intact graphene electronic structure, which acts as a source of electrons in catalytic reaction steps (Rodriguez-Reinoso, 1998).

2.4.1.2 CARBON FUNCTIONING AS A SUPPORT

Carbon materials are exceptional because of the many different forms of carbon that area available and the complex functions that they accomplish. They are also associated with a

unique family of supports (Bansal *et al.,* 1988; Stoeckli, 1990). This elemental atom can be classified initially with the sp^2 hybridised chemical bonding in the orderly structure of the graphitised carbons, and the disordered turbostratic carbons similar to activated carbon. The sp^3 hybridised configuration in diamond, and the different allotropic forms of elemental carbon possessing distinct bulk and surface properties, can be tailored to the desired character.

There has been a rapid increase in the past three decades with regard to the use of the various forms of carbon as heterogeneous catalyst supports. In the midst of these are graphite and diamond as well as activated carbon. This support has received importance because of its properties including porosity, surface area and chemical nature, in addition to its mechanical resistance, stability and inertness (Dandekar *et al.,* 1999).

The features that make carbon an excellent material for catalyst supports are its chemical inertness, and stability in an oxidising and reducing environment (at temperatures below 400^{o}C). Carbon atoms demonstrate mechanical resistance and have a high surface area (Stiles, 1987). It is also possible to modify the surface with functional groups (Tamai *et al.,* 2006).

2.4.2 CARBON SUBSTRATES

2.4.2.1 ACTIVATED CARBON

The synthesis of activated carbon can take place by means of two different methods, *viz*. physical or chemical activation or a combination of both of them. The physical activation method involves carbonization of the raw material and the subsequent activation of the carbon at high temperature, in carbon dioxide or a steam atmosphere. The chemical activation method involves the carbonization of the raw material previously impregnated with a chemical agent (Moreno-Castilla *et al.,* 2001).

Activated carbons have well developed porous structures and a large internal specific surface area, with values close to 1000 m^2/g reported (Okada *et al.,* 2003). The high surface area and porous structure of these material enables it to adsorb gases and compounds dispersed or dissolved in liquids. There have been many attempts to

functionalize the surfaces of this material with suitable reagents. The precursors that have been used to modify the surface of activated carbon material include concentrated nitric or sulphuric acid, sodium hypochlorite, permanganate, bichromate, hydrogen peroxide, transition metals and ozone-based gas mixtures (Rios *et al.,* 2003). The functionalization of the activated carbon enhances its adsorption of heavy metals such as Hg^{2+}, Zn^{2+}, Cd^{2+} and Pb^{2+} ions due, to the presence of surface –SH and –NH groups (Rios *et al.,* 2003).

2.4.2.2 CARBON NANOTUBES

Carbon nanotubes (CNTs) are tubular structures made up of carbon atoms, having diameters of nanometre order but lengths in micrometers. CNTs display unique properties *viz:* that are stronger than steel, harder than diamond, electrical conductivity higher than copper and thermal conductivity higher than diamond. Chemical vapour deposition (CVD) is the most popular technique to prepare carbon nanotubes because of its low set-up cost, high production yield, and ease of scale-up (Kumar *et al.,* 2010; Zhu *et al.,* 2011).

Carbon nanotubes are a class of porous materials which have interesting structures and properties and as such, they have widespread application. They were originally formed on a carbon electrode of an arc discharge apparatus that was utilised in the mass production of C_{60} and C_{70}. They are made up of sheets of graphene and are structurally quite stable. Since these are void particles, they can be rolled up in a helical fashion and their ends can be sealed with fused pentagonal rings as demonstrated in Figure 2.3 (Langley *et al.,* 1999).

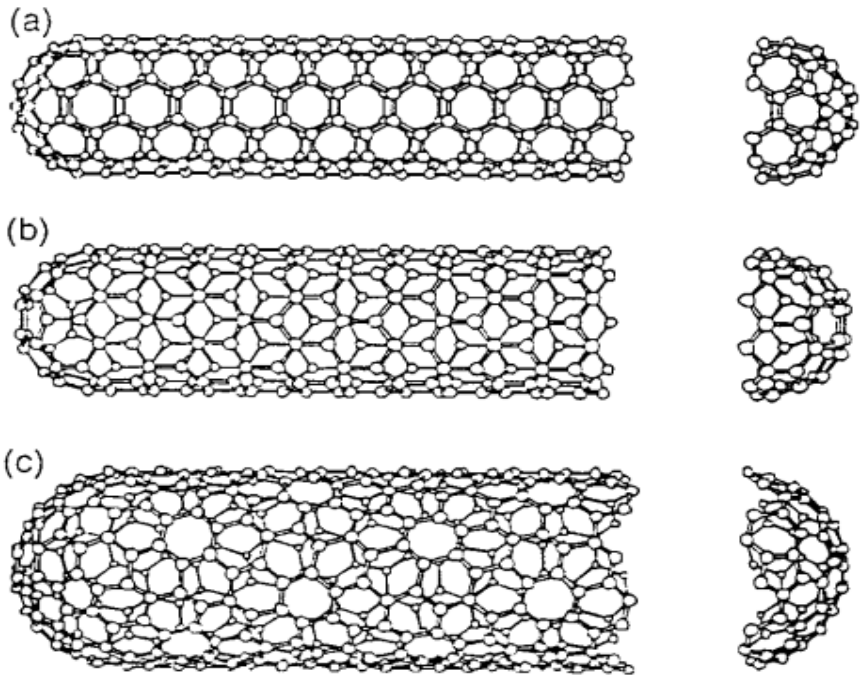

Figure 2.3: Representation of different types of single-walled carbon nanotubes: (a) arm-chair configuration; (b) zig-zig configuration; (c) chiral configuration. (Dresselhaus et al., 1995)

Carbon nanotubes can be considered single- or multi–walled nanotubes with scroll-like structures and internal diameters ranging from ca. 2 nm for the inner tubes of multi-walled species, to ca. 30 nm for the larger species. These materials have an exceptionally high aspect ratio and they can be normally 1 mm or even longer in length. They have high structural anisotropy, even weight ratio and a small number of defects. As a result they are considered the toughest fibre that has been identified to date.

Carbon nanotubes are comprised of cylindrical carbon molecules, with properties that make them valuable in extremely small scale electronic and mechanical applications as demonstrated in Fig 2.3. They demonstrate unusual strength and unique electrical properties, and are good conductors of heat (Iijima; 1991).

2.4.2.3 FULLERENES

The fullerene molecule, C_{60}, was fabricated in 1985 and is related to the study of nanocarbons (Kroto *et al.,* 1985). This molecule has a shape that resembles a soccer ball and consist of 60 carbon atoms connected together to form a perfect, one-atom thick, hollow sphere. This involved interaction of the C-C bonds through bent sp^2 hybridised

carbon atoms. This resulted in a strained structure with good reactivity. A schematic diagram of a C_{60} molecule is shown in Figure 2.4.The carbons atoms (all sp^2 hybridised) are mutually connected to form 12 pentagons and 20 hexagons. Kratschmer *et al.*, (1990) reported the synthesis of fullerenes using a simple method to produce isolable quantities of the C_{60}.

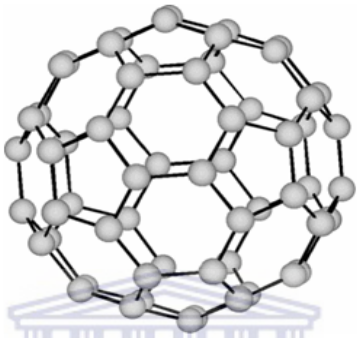

Figure 2.4: Schematic diagram of a C_{60} molecule (Ajie *et al.,1990).*

2.4.2.4 TEMPLATED CARBON MATERIALS

The template methodology is an emerging development and one such example is the use of this method to make Mesostructured Silica Materials (MSM). This material has a rigid structure and a well–structured pore network. They make excellent templates for the production of novel materials with a well ordered structure and exceptional properties, e.g. to make noble metal nanowires and networks, conductive polymer nanofilaments or mesoporous carbons.

Carbons have found widespread technological applications in the role of the absorption of large molecules, as a catalytic support in fuel cells or for energy storage in double – layer capacitors and as porous carbons. The porous carbons with a narrow pore size distribution (PSD) in the mesopore range (2–50 nm) have an added advantage with regards to classical active carbon because of the broad PSD and the presence of many micropores. The synthesis of mesoporous carbons with these features was made using MCM–48 silica as a template (Ryoo *et al.,* 1999). It has been reported elsewhere that mesoporous carbons were prepared using various types of templates such as SBA–15 and

HMS. The pore network, morphology or particle sizes of these templated carbons are a replica of the MSM which is used as the template (Fuertes *et al.,* 2003; Sang *et al.,* 2011).

The templating approach has been employed to produce mesoporous carbon and involves the infiltration of carbon precursors such as furfuryl alcohol, sucrose, divinylbenzene, polyacrylonitrile, cyclodextrin, phenol, resorcinol, and formaldehyde into the pores of the inorganic frameworks. Carbonization of the precursors and subsequent removal of the inorganic templates, results in porous carbons with templated pore structures

The various templates that have been utilised include colloidal silica, zeolites, and mesoporous silica. Mesoporous silica is the most common template due used to its controllable pore size and structure. This template is prepared by means of a mutual assembly of surfactants and silicates into hexagonal, cubic, lamellar, and other ordered lyotropic liquid–crystalline mesophases. The subsequent removal of the surfactants produces silica with ordered mesoporous channels and controllable 2–30 nm diameter pore sizes (Hampsey *et al.,* 2005)

The use of different surfactant templates, periodic mesoporous silicas (PMSs) with various pore sizes and structures such as MCM–41 (2D hexagonal), MCM–48 (cubic), HMS (wormlike), SBA–1 (cubic), SBA–3 (2D hexagonal), and SBA–15 (2D hexagonal), have been investigated (Vinu *et al.,* 2006). In contrast to microporous zeolites, the pore sizes of PMS materials can be controlled in the range of 2–30 nm, simply by choosing an appropriate surfactant template and the addition of a micelle swelling agent.

The addition of an organic component either on the pore surface or in the framework, improves the physical and chemical properties of PMS materials. It is also an efficient way to functionalize surfaces, thus exploiting the opportunity to produce novel materials.

The post grafting of organosilanes on the surface of MCM–41 increases its hydrothermal stability and improves its hydrophobicity. It also ensures that the surface-functionalized materials are utilized as potential adsorbents for the control of volatile organic compounds present in industrial waste streams (Zhao, 2006).

The synthesis of porous carbons is usually achieved through a sequence of stages. This includes the carbonization of precursors of natural or synthetic origin, followed by activation. The templated synthesis of ordered mesoporous carbons has significantly enhanced the area of porous materials. The unique properties exhibited by these materials make them suitable as adsorbents, catalyst supports, and materials for advanced electronics applications. This material was first prepared by carbonizing organic polymers under an inert atmosphere. The major drawback in the preparation of carbons in this way was that they displayed irregular shapes, broad pore size distributions, etc. The template method has been remarkable in giving materials with specified morphology and microstructure (Sakintuna *et al.*, 2005).

2.4.2.5 MESOPOROUS CARBON MATERIALS

The structure of mesoporous carbon nanoparticles (MCN) has been investigated using various characterization techniques, including the scanning and transmission electron microscopy (SEM and TEM), powder X-ray diffraction (XRD), and N_2 sorption analysis. The TEM images of the synthesis of MCM–48 type mesoporous silica nanoparticle (MSN) material as the structure-directing template via a modified Stober method is illustrated in Figure 2.5 (Kim *et al.*, 2008). The TEM micrographs of the MCN material consist of monodisperse spherical nanoparticles (100 – 200 nm). The TEM micrograph as indicated in Figure 2.5a demonstrates the exact replication of the whole particle morphology (spherical particles). In addition, a tetragonal *I*41/*a* (or lower) mesoporous structure, which is the replication of the cubic *Ia*-3*d* porous morphology of the MSN template, was also observed in Figure 2.5b. The high magnification TEM images of MSN and MCN materials (Figure 2.5, panels c and d) confirmed the highly ordered mesoporous structures throughout the entire particle of these materials.

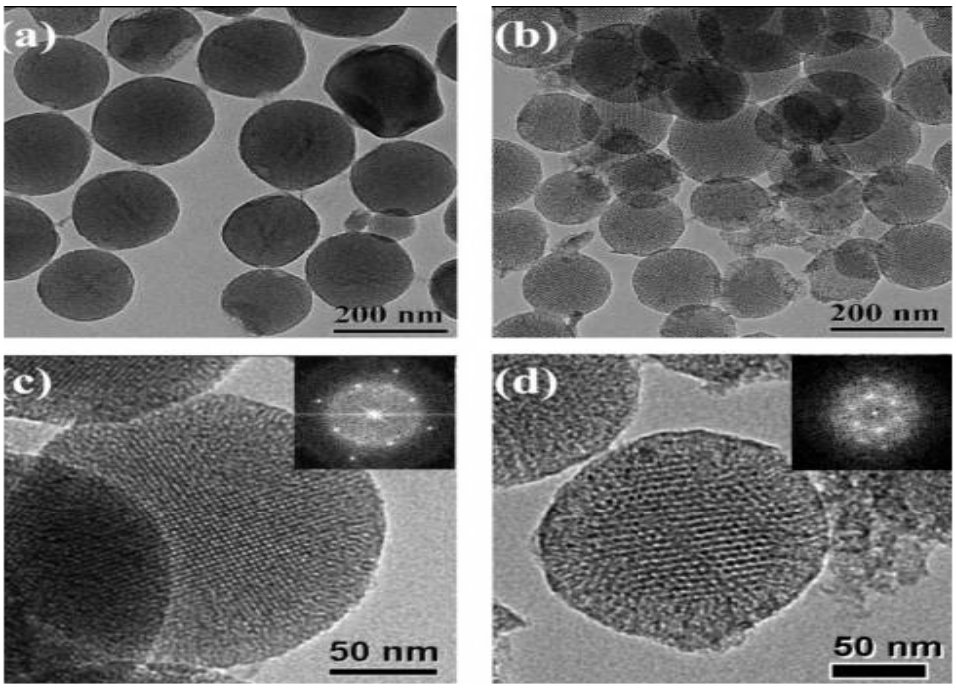

Figure.2.5: Low-magnification TEM images of (a) mesoporous silica MCM-48 nanoparticles and (b) mesoporous carbon nanoparticle (MCN) materials. High-magnification TEM images of (c) MCM–48 nanoparticle and (d) MCN material with the corresponding Fourier diffactograms (insets) (Kim *et al.*, 2008).

The XRD patterns of MSN and MCN in Figure 2.6 shows the successful change from the cubic *Ia*-3*d* (MCM–48 type) to the tetragonal *I*41/*a* (or lower) mesoporous structure after the carbon replication process. The N_2 sorption isotherm of MCN (Figure 7b) exhibited two capillary condensation steps at P/P_0 = 0.18 – 0.3 and > 0.95, which could be attributed to the N_2 condensation that took place at the internal mesopores and the interparticle voids, respectively.

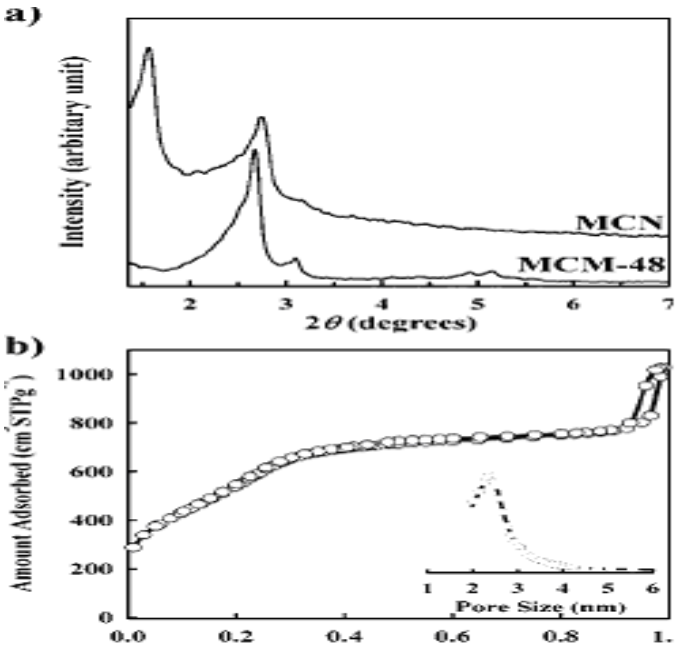

Figure.2.6: (a) Powder XRD patterns of MCN (top) and the calcined, MCM–48 type MSN silica template (bottom). (b) N_2 sorption isotherm and the pore size analysis with adsorption branch using the BJH algorithm (inset) of MCN.

It was found that MCN has large BET surface area (~2000 m^2/g) and pore volume (1.2 cm^3/g) as shown in Table 2.1. The BJH pore size distribution showed an average pore diameter of 2.4 nm (Kim *et al.,* 2008).

Table 2.1: Structural Properties of MCM–48 Mesoporous Silica Nanoparticles and Ordered Mesoporous Carbon Nanoparticle MCNs from Nitrogen Adsorption Data (Kim *et al.,* 2008)

Sample	$S_{BET}(m^2g^{-1})$	V_t (cm^3g^{-1})	BJH(nm)
MCM – 48	1278	0.96	2.3
MCN	2034	1.2	2.4

2.4.2.6 GRAPHITIC MESOPOROUS CARBON

The synthesis of porous carbons with a graphitic framework has been described in the literature. They have been prepared using traditional techniques such as: (a) catalytic graphitisation of carbons obtained from polymeric gels, (b) imprinting of silica nanoparticles into the matrix of a graphitisable carbon precursor (Ryoo *et al.,* 1999) or (c) infiltration of a graphitisable carbon precursor into the porosity of mesostructured silica (Ryoo *et al.,* 1999), which is used as template. Hollow graphitic carbon nanoparticles and carbon nanocoils were prepared by carbonising resorcinol–formaldehyde gels doped with cobalt and nickel salts (Hyeon *et al.,* 2003). These metals aid in the graphitisation process and they facilitate the formation of graphite crystallites at fairly low temperatures (~ 900 ^{o}C) because they act as catalyst.

The combination of good electronic conductivity and a large accessible surface area in carbons has led to their use in certain emergent applications, such as electrodes in double-layer electrical capacitors or as catalytic supports in low-temperature fuel cell systems. Porous carbons that are synthesised from non-graphitisable materials do not display high electrical conductivity, even after heat treatment at high temperatures. Even though graphitisable carbons have been synthesised from polymers (i.e. poly-vinyl chloride), aromatic hydrocarbons (i.e. naphthalene, phenantrene, etc.) or mesophase that demonstrates good electrical conductivities, these materials are not suited for developing porosity using activation procedures when preparing activated carbons. The reasons stem from the fact that these carbons are impervious to gasifying agents that prevent the creation of pores.

Zhao *et al. (*2003) has reported the preparation of graphitic mesoporous carbon by imprinting colloidal silica particles into mesophase pitch. The specific surface area was 240 m^2g^{-1} and a pore volume of 0.7 cm^3g^{-1} (pore size ~ 17 nm) and was reported for carbons obtained after carbonisation and subsequent heat treatment at 2400 ^{o}C.

The average d spacing (0.34 nm) for these carbons provides evidence that graphitisation has been achieved as determined by the Bragg equation. The surface areas for carbon coils and hollow carbon particles were 318 m^2g^{-1} and 88 m^2g^{-1} respectively. These

materials provide an excellent support for Pt/Ru electrocatalysts in DMFC (direct methanol fuel cells) systems.

The template is used to obtain the pore network of the carbon that is an inverse replica of the inorganic material. In this way the porosity of the carbon framework is controlled and commonly employed to produce non-graphitisable mesoporous carbon, utilizing different types of mesoporous silica materials (MSM) as templates. The careful selection of an appropriate template for the synthesis of carbons can alter the structural characteristics (i.e. surface area, pore volume, pore size, particle size, morphology, etc.). A graphitic framework can be achieved if the porosity of the template is infiltrated by a graphitisable carbon precursor.

Ordered graphitic carbons were prepared by infiltrating the pores of mesostructured silica materials (i.e. MCM–48 and SBA–15) with acetanaphthene. The infiltrated material was heated at 750 ^{o}C under pressure in an autoclave and then heated at 900 ^{o}C under vacuum. The resultant carbon displayed a turbostratic structure with a d_{002} spacing of 0.36 nm (Kim *et al.,* 2003).

The preparation of porous carbons with graphitic framework and a large surface area with an accessible porosity made up of mesopores has been made. The preparation of this material involved infiltrating the pores of a mesostructured silica with a solution containing a polymer under ambient conditions (temperature and pressure), that was converted into a graphitisable carbon after the carbonisation step. The subsequent heat treatment of the graphitisable carbon at high temperature (2300 ^{o}C) produced a porous carbon with a well-developed graphitic order. Polyvinyl chloride (PVC) was used as the polymeric material to infiltrate the two different MSM templates, i.e. well-ordered silica (SBA–15) and silica with a wormhole pore structure (MSU–1) (Fuertes *et al.*, 2004).

2.5 NANOSTRUCTURED ELECTROCATALYST FOR PEM FUEL CELLS

Nanostructured carbon materials have been identified as an excellent support material for Pt – based electrocatalysts (Perathoner *et al.,* 2007). This is based on the following conditions (i) the materials possess a high surface area to enable a high distribution of the

nanosized catalyst; exceptional crystallinity or low electrical resistance to allow the flow of electrons during the electrochemical reaction; an appropriate pore structure for sufficient fuel contact and the liberation of byproducts; and ensuring excellent contact between the catalyst nanoparticles and the carbon support (Perathoner *et al.*, 2007).

Carbon materials that possess nanostructures have been used to obtain highly developed electrocatalysts as a result of these remarkable characteristics. The factors that have been established to ensure this development are as follows: (Perathoner *et al.*, 2007)

1. This material has demonstrated outstanding electrical properties that make use of the charge of the supported metal particles.
2. The existence of an ordered structure allows for a better mass-transfer and three phase boundary.
3. There is also a chance of crystallographic rearrangement of the supported metal nanoparticles.
4. The limitations created within nanotubes,
5. The likelihood of improving the performances and decreasing sensitivity to poisoning by the combination of oxides with carbon, and
6. The opportunity to build structures on the nano-, meso-, and microscale.

The structural design of carbon and the nature of metal – carbon interactions are influenced by the carbon framework. This can create an improved three-phase boundary (gas–electrode–electrolyte) and also facilitate interaction between metal particles and the conductive carbon substrate. This enables an efficient chemical–to–electrical conversion that is essential for the development of PEM fuel cells (Perathoner *et al.*, 2007).

2.6 PLATINUM DEPOSITED BY ORGANOMETALLIC CHEMICAL VAPOUR DEPOSITION (OMCVD)

The deposition of platinum by chemical vapour deposition (CVD) on solid supports has advanced considerably, because of the good electrical conductivity and catalytic properties displayed by this element. Organometallic chemical vapour deposition (OMCVD) is a technique whereby a metal containing precursor, typically an organometallic complex is vapourized and that undergoes thermal decomposition. This is

followed by deposition onto the substrate to form a metal layer. Metallic particles are formed as a result of heating the substrate above its stability range, thus causing the decomposition of the organometallic species. The distinct advantage of using CVD techniques is that the pyrolysis temperature in OMCVD is much lower than in other techniques. This method is fast, in contrast to the liquid impregnation technique. In addition, surface poisoning and material transformation is eliminated. This method is very efficient and produces deposits of high quality. The major disadvantage of using OMCVD is the possible incorporation of impurities due to non–exhausted residues and in certain cases poor adhesion of the film.

The OMCVD methodology involves the vapourization of the precursor at low temperature and reduced pressure in order to obtain a precursor vapour pressure for film deposition, thereby enabling the metal to deposit on a substrate surface at a higher temperature by adsorption and thermal decomposition of the precursor (Thurier *et al.*, 2008).

The different stages of the OMCVD process are outlined below and are depicted in Figure 2.7 (Thurier *et al.*, 2008).

- Convection of the gaseous reagents
- Diffusion of the reagents towards the substrate
- Adsorption of the reagent onto the substrate
- Chemical reaction of the adsorbed species producing nuclei and further reaction to give a metal film
- Desorption of the gas products of the reaction
- Diffusion of these products through the boundary layer
- Gas evacuation of the system

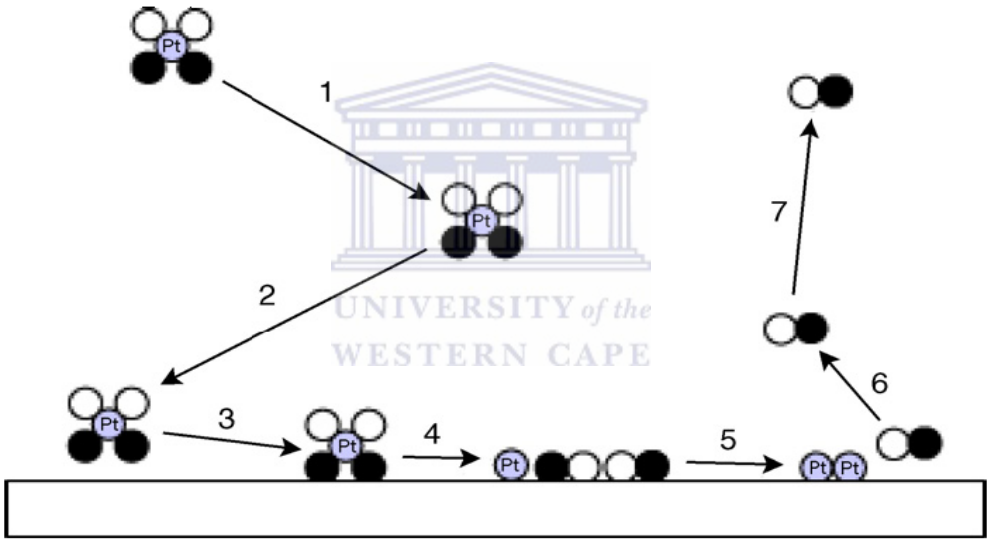

Figure 2.7: Stages of a traditional MOCVD process (Thurier *et al.,* 2008).

2.7 ELECTROCHEMICAL ACTIVITY USING CYCLIC VOLTAMMETRY

The CV curves of mesoporous active carbon (MPAC) and Vulcan XC–72R are illustrated in Figure 2.8 (a) and (b (Hwang *et al.,* 2009). These measurements were performed in both sulphuric acid solution (solid lines), and $K_3[Fe(CN)_6]$ (dash lines). The bigger area indicates the larger capacitance. This means that ions are more strongly adsorbed on the surface of an electrode and this causes an inference with specific reactions. The

occurrence of solvated $K_3[Fe(CN)_6]$ results as shown by the appearance of a redox couple as electrons are transferred at the interface of electrode and electrolyte. The potential difference between the oxidation peak and reduction peak should be 59 mV for an ideal electrolyte. The potential difference that is measured is more often larger than that. A higher the peak current would result in more electrons moving, thus yielding better electrochemical activity. In Fig 2.8a, MPAC demonstrates low current performance in sulphuric solution in comparison to the solution with solvated $K_3[Fe(CN)_6]$ with a potential difference close to 100 mV. There are no other reaction peaks present in both electrolytes. The results shown in Fig 2.8b indicate that MPAC would be a good electrode material for electrochemical applications. Fig 2.8b illustrates the Vulcan XC–72R which, despite the total current performance being higher than that of MPAC, a significant capacitance effect. The potential difference is smaller than 59 mV, as a result of the adsorption effect. This means that the current contribution of a redox couple appears as a result of the reactants adsorbed on the electrode surface and not from fresh reactants continuously diffusing from electrolyte.

This property is not necessary for an electrode material. In both instances, the top part at high potential represents the formation of oxygen, and the arrow-marked peaks signify the reduction of oxygen produced. There is an additional tiny redox couple noticed at ~ 0.1 V in $K_3[Fe(CN)_6]$ electrolyte. This is due to the presence of the functional groups or impurities in Vulcan XC–72R. (Hwang *et al.*, 2009)

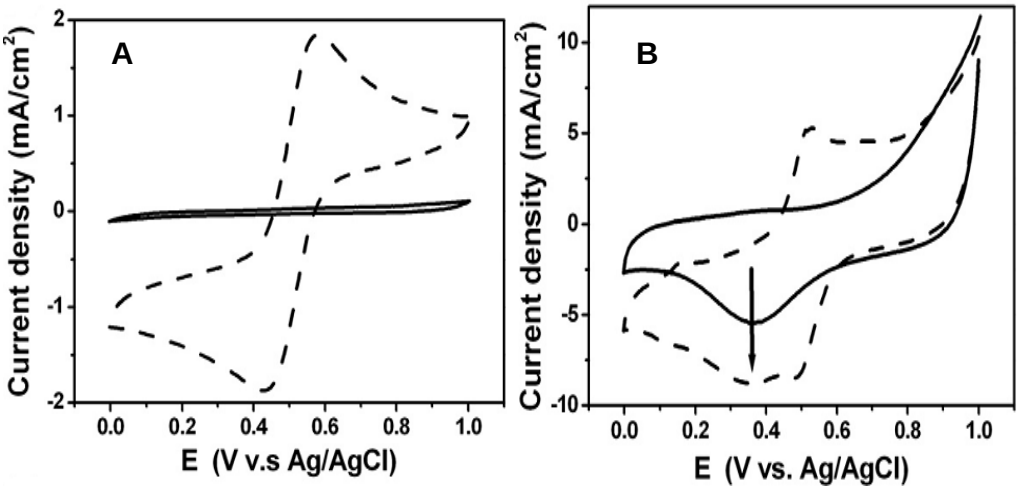

Figure 2.8: Cyclic voltammetry analyses of (a) MPAC and (b) Vulcan XC-72R. Measurements were conducted in electrolytes of 1 M H_2SO_4 (solid line) and 1 M H_2SO_4 plus 10 mM $K_3(Fe(CN)_6)$ (dash line) with scan rate of 10 mV/s (Hwang *et al.,* 2009).

Carbon- and graphite-supported platinum catalysts have been frequently applied to fuel cells. The increase of metal particles and the deposition of carbon species or oxidation of the metal can deactivate the catalyst during reaction. Cyclic voltammetry (CV) provides information about the surface area of the platinum particles and particle growth. This technique has been used to characterize a catalyst surfaces before and after reaction in the liquid phase. The ability to detect fractions of a monolayer of oxygen or of organic adsorbates is possible, thus making this method surface–sensitive. The cyclic voltammograms of the catalysts for determination platinum surface area are shown in Fig 2.9A..

Figure 2.9A shows the cyclic voltammogram obtained on a freshly reduced platinum catalyst used to determine the surface area. This Figure is typical for platinum. For instance the deposition and oxidation of hydrogen atoms and the adsorption and reduction of oxygen atoms, are quite distinct. Figure 2.9B shows the cyclic voltammogram of the graphite support.

The portion of exposed platinum atoms on the catalyst was reduced in the liquid phase and this can be observed from Fig. 2.9C. The net effect of this reaction on the portion of exposed platinum atoms can be shown by comparing Fig. 2.9C and D. It is quite easily

seen that the tiny proportion of exposed platinum atoms has strongly decreased after reaction. The cyclic voltammogram of the used catalyst strongly resembles the cyclic voltammogram of the graphite support as shown in Figure 2.9B (de Bruijn *et al.,* 1992).

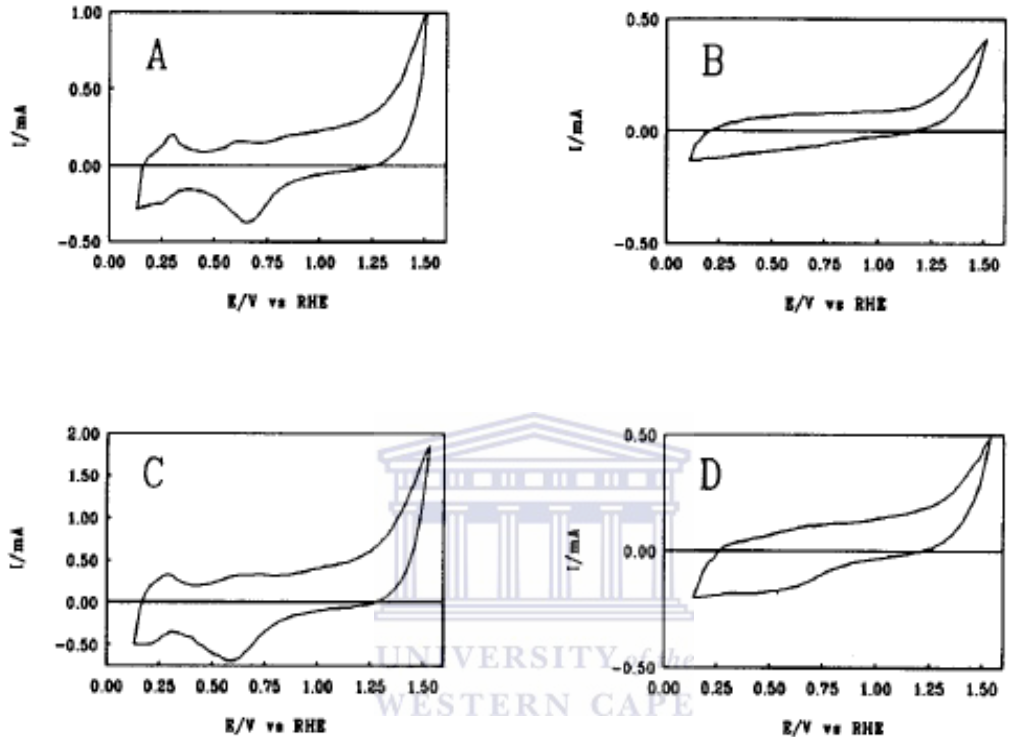

Fig. 2.9: (A) Cyclic voltammogram of a freshly reduced 4.9 wt.% platinum/graphite catalyst; scan rate 1 mV s-1 (B) Cyclic voltammogram of graphite support before ion exchange with platinum ions; scan rate 1 mVs-1. (C) Cyclic voltammogram of a 4.9 wt.% platinum/graphite catalyst after reduction in liquid phase at T = 363 K, pH 7, for 1 h with molecular hydrogen followed by addition of 0.2 M methyl a-Dglucoside. (D) As C followed by oxidation of methyl a-D-glucoside with molecular oxygen at T = 323 K, pH 9, for 20 h (de Bruijn *et al.,* 1992).

2.8 CARBON SUPPORTS FOR FUEL CELL CATALYSTS

One of the many applications of carbon is to use it as a catalyst support for fuel cells. Low temperature fuel cells are receiving increasing interest as a method of generating electricity by direct electrochemical conversion of hydrogen, ethanol, methanol, and oxygen into water and carbon dioxide. In low temperature fuel cells platinum and

platinum alloys are used as anode and cathode catalyst. The reaction surface of a catalyst increases as the activity of the catalyst increases. The catalyst particles should be reduced in diameter to increase the surface area. The decrease in particle size can result in a decrease in the specific activity of metal nanoparticles. An effective support for a fuel cell catalyst is that it should have a high surface area this can be achieved through high porosity and sufficient electrical conductivity, so as to facilitate the flow of electrons. It is essential that carbon supports have a high percentage of mesopores, in the 20 to 40 nm region. This will offer offering a high accessible surface area to the catalyst and to monomeric units of the Nafion ionomer so as to boost the diffusion of chemical groups. The activity of the catalyst is influenced by the support material, given that the catalyst bonds to the support. These effects can be described in two ways. The electronic structure of the catalyst can be modified by the support material. The reaction characteristics of the active sites present on the surface of the catalyst might be affected by the electronic effect. The shape of catalyst particles may perhaps be modified by the support material. The stability of a catalyst in the development of new substrates in the area of fuels cells is needed. Factors such as high surface area, porosity and electrical conductivity, and corrosion resistance contribute to selecting a good catalyst.

Carbon blacks have been extensively used as catalysts in low–temperature fuel cells and are produced by the pyrolysis of hydrocarbons, such as natural gas or oil fractions from petroleum processing. The ash content of carbon black is substantially low, mainly because of the characteristics of the starting materials (Antolini, 2008). The carbon blacks are fabricated by the oil furnace processes and acetylene processes (Antolini, 2008). The furnace black process is the main method of production and in this process the starting material is fed to the furnace and burned with a controlled supply of air at about 1400 ^{o}C. Oil–furnace carbon black (eg. Vulcan XC–72) supports for platinum catalysts in low temperature fuel cells has gained momentum and has been used by many (Antolini, 2008). Vulcan XC–72 is not a well defined oil furnace black material as has been reported, since the particles are not mono–disperse. High surface area graphite (HSAG) that possess a surface areas of between 100 – 300 m^2g^{-1} have been attractive as a support material for precious metal catalysts. An additional support material used by catalyst manufacturers,is graphitized carbon black. It has been reported that this material can be acquired by recrystallization of spherical carbon black at 2500 to 3000 ^{o}C.

The deposition of metals onto carbon supports by impregnation methods indicates that the specific surface area of the carbon support does not affect the Pt dispersion (Antolini, 2008). It was demonstrated that the Pt particle size decreased when increasing the specific area of the carbon black. The acetylene black has a greater number of pores with a diameter of 3 – 8 nm than does oil–furnace black supports (Antolini, 2008; Grigoriev *et al.* 2011; Zeng *et al.* 2008).

2.9 CHARACTERISATION TECHNIQUES

2.9.1 FOURIER TRANSFORM INFRARED (FTIR) SPECTROSCOPY

Infrared spectroscopy has been applied to characterise mesoporous silica throughout the synthesis process (Osswald, 2006). Chemical bonds are continuously stretching and bending, lengthening and contracting. When the frequency of the light and vibration are equal the bond absorbs energy as it is irradiated. Whilst infrared energy is absorbed by a molecule, the molecular vibration increases in amplitude with a frequency matching that of the light. The light frequency absorbed by the molecule corresponds to a specific molecular motion. This kind of molecular motion in each sample is measured by its characteristic infrared absorption.

The main absorption band in amorphous silica occurs between 1300 and 800 cm^{-1} and consists of several bands as shown in Table 2.2. The most dominant band is assigned to the asymmetric stretching vibrations of Si–O–Si in the range of 1130 – 1060 cm^{-1}. On the high frequency side of this band there is a shoulder, which is related to skeletal stretching vibrations. The shoulder at the low frequency side is assigned to the Si-O stretching vibration of surface silanol groups. A second, very weak band related to the silanol vibration can be observed in the range of 900 – 880 cm^{-1}. This band is assigned to the bending vibration of the silanol group (Osswald, 2006).

Table 2.2: FT-IR band assignment for silicate solutions (Osswald, 2006)

Wavenumber (cm^{-1})	**Assignment**
1225–1180	Si-O-Si asymmetric stretching vibration, (LO_3 mode)
1175–1138	Skeletal Si-O stretching vibration
1126–1078	Si-O-Si asymmetric stretching vibration (TO_3 mode)
955–940	Si-O stretching vibration of surface silanol groups
895–880	Si-OH bending vibration

2.9.2 X–RAY DIFFRACTION

Powder X ray diffraction is a technique that can be used to study the crystallinity and atomic structure of materials. This technique can be used to evaluate the particle size of Pt and crystalline structures of the Pt/C catalyst. In this study it was used to obtain the particle sizes using Scherrer equation and the XRD analysis (Shimura, 1989).

The crystallite size can be determined by measuring the broadening of a particular peak in a diffraction pattern associated with a particular planar reflection from within the crystal unit cell. The particle size is inversely proportional to the half – width at half maximum of an individual peak. Therefore a sharp peak will result in a larger crystallite size (Shimura, 1989).

The width of the diffraction peak is associated with the size of the crystals and is given by Scherrer equation as shown in equation 2.1:

$$\mathbf{d = 0.9\ \lambda_k / (B \cos\theta_{max})} \quad \text{.....(2.1)}$$

where d = particle size (nm)

λ_k = wavelength (Cu-Kα, λ = 1.5406Å)

θ_{max} = half the angle of diffraction (2θ)

B = peak width at half peak height (radians)

The lattice parameter (α) as shown above can be determined by equation 2.2:

$$\alpha_{fcc} = 2^{½} \lambda_k / \sin\theta_{max} \quad \text{.....(2.2)}$$

2.9.3 SCANNING ELECTRON MICROSCOPY (SEM) / ENERGY DISPERSIVE X-RAY (EDS) SPECTROSCOPY

Scanning electron microscopy (SEM) is a complex imaging technique capable of producing three-dimensional profiles of material surfaces. It was used in this study to extract quantitative and qualitative information pertaining to agglomerate size/shape, particle morphology, and surface appearance of supported nanophase electrocatalysts.

The standard operation in SEM involves the interaction of an accelerated highly mono-energetic electron beam, originating from a cathode filament, with the atoms at a sample surface. The electron beam is centred onto a fine probe and then scattered over the sample surface. These scattered electrons are collected by a detector, modulated, and amplified. This produces an exact reconstruction of the sample surface and particle profile (Cherstiouk *et al.,* 2003).

The technique is based on the fact that every element has a unique atomic structure such that X-rays characteristic of different atomic structures are readily distinguishable from one another. In EDS, the incident electron beam excites an electron in an inner shell, causing its ejection and the formation of an electron hole in the electronic structure of the atom. An electron from a higher-energy (outer) shell fills the hole, and the difference in energy between the higher-energy shell and the lower-energy shell is released as X-rays. The X-rays thus released are analyzed by means of an energy-dispersive spectrometer. EDS systems are commonly found with SEM, as well as with TEM instruments.

2.9.4 HIGH RESOLUTION TRANSMISSION ELECTRON MICROSCOPY (HRTEM)

This technique examines the internal structure of solids and provides information about the micro – structural detail. TEM is often used in the determination of average particle size, particle shape, and particle size distributions of supported nanophase electrocatalysts. In this investigation, TEM was utilized in the direct examination of supported nanophase electrocatalysts,:nanoparticle size and nanoparticle size distribution.

In HRTEM operation, a narrow electron beam originating from a tungsten filament is concentrated onto ultra-thin sample surfaces using a series of magnetic lenses. The electrons interact with sample atoms while penetrating the thin sample structure leading to the transmittance of electrons and the production of secondary electrons. Secondary electrons pass through an aperture to produce an image on a fluorescent screen. For carbon-supported metal electrocatalysts, metal particles appear as dark areas and low atomic weight carbon supports appear as light areas in the resultant micrographs due to differences in electron transmittance with increasing atomic weight. The obtained information is often complemented by quantitative information such as total surface area and porosity (Cherstiouk *et al.,* 2003).

2.9.5 BRUNAUER, EMMETT AND TELLER (BET) SURFACE ANALYSIS

This method can be used for measuring specific surface area of particles, which is based on the theory stated by Brunauer, Emmett and Teller. This involves heating the sample under vacuum to remove adsorbed gas from the sample. Subsequently the sample is cooled by liquid nitrogen (73K). The introduction of an inert gas (like nitrogen) over the surface of the cooled sample, results in gas being adsorbed. As the process temperature and the volume of chamber is constant, by varying the gas pressure, the pressure that adsorption and desorption of gas gives an isotherm can be found due to the ideal gas law:

$$PV = nRT$$

where P is absolute pressure, V is volume, n is number of atoms, R is the gas constant (8.13 J/K.mol) and T is absolute temperature of gas.

In the basic operation, solid samples are placed in an evacuated sample holder at constant temperature ≈ 110 °C. The sample holder is filled with helium to flush contaminating gases from the sample surface and pores. The helium is then purged from the system. Evacuated samples are cooled to -196 °C in a liquid N_2 bath while the sample holder is filled with ultra-pure N_2 gas. Pressure within the sample holder is monitored over time, and then rapidly reduced to reach an equilibrium state where the quantity of gas adsorbed onto the surface is equivalent to the quantity of gas removed from the gas phase. By plotting the quantity of N_2 adsorbed versus the equilibrium pressure an adsorption isotherm is obtained, which together with the BET equation can be used to determine the sample surface area. This adsorption isotherm can be defined as the plot of the dependence of the fractional coverage of surface-adsorbed molecules on pressure, at constant temperature. The BET equation can be given as follows: (Webb, 1997)

$$\frac{1}{W[(P_o/P)-1]} = \frac{1}{W_m C} + \frac{(C-1)}{W_m C}\frac{P}{P_o} \quad \text{..... (2.3)}$$

where W is the weight of N_2 adsorbed at a given relative pressure (P/P_o), W_m is the weight of gas producing monolayer coverage, and C is a constant related to the heat of adsorption.

Pore size, pore size distribution, and pore volume of supported nanophase electrocatalysts can be determined using the Barrett-Joyner-Halenda (BJH) method (Webb, 1997).

2.9.6 THERMOGRAVIMETRIC ANALYSIS (TGA)

The thermogravimetric analysis (TGA) technique examines the variation of mass loss/gain that a material undergoes when this material is subjected to temperature change (Haines, 1995). This variation of mass is usually a loss of mass, arises since, during the heating process, different chemical reactions occur, where volatile compounds are formed. These reactions indicate combustion, dehydration, decomposition, etc. (Brown, 1998; Tusi *et al.* 2011).

2.9.7 CYCLIC VOLTAMMETRY (CV)

Cyclic voltammetry (CV) can be used to investigate electrode surface reactions, the behavior of electrochemically-active species, and to examine the quality of electrocatalysts. CV provides information on the thermodynamics of redox processes and the kinetics of heterogeneous electron-transfer reactions. One of the advantages is that it can probe surface reactions in-situ under well-controlled conditions, giving insight into the catalytic mechanisms and the catalytic activity of nanophase electrocatalysts (Steigerwalt *et al.,* 2001).

The process involves cycling a potential applied to an electrode immersed in a inert electrolyte solution, containing an analyte species, through a defined potential range and measuring the resultant current. The measured current is a result of electron flow through the electrochemical circuit and is due to diffusional mass transfer of electro-active species as migration and convection are minimised. The applied potential is swept back and forth between two designated potentials, at a constant rate, by a potentiostat. Typically, a three-electrode system consisting of a working electrode, reference electrode, and counter electrode is used. The working electrode is the electrode of interest at which potential is applied. The reference electrode experiences zero current and has a known standard potential against which all other potentials are measured. The role of the reference electrode is to provide a fixed potential which does not vary during the experiments (Steigerwalt *et al.,* 2001; Tusi *et al.* 2011; Alegre *et al.* 2011).

2.10 SUMMARY OF THE CHAPTER

The literature survey has outlined the synthesis of mesoporous silica and mesoporous carbon materials and illustrates the flexibility in designing chemical and physical properties according to a certain requirement. It illustrated their remarkably wide range of applications. The use of a suitable silica template as a sacrificial template for the synthesis of the carbon analogue in catalysis will depend on a systematic approach to the synthesis as well as control of the chemistry of the carbon surface.

In summary, in situ carbonisation of organic compounds, carbon nanocomposites and carbons will give materials with a well developed pore structure, and high surface areas.

Furthermore, highly ordered mesoporous carbon materials are now accessible, by templated synthesis with a rich variety of structures, using mesoporous silica as templates. The templated synthesis of an ordered mesoporous carbon is a remarkable achievement in the field of porous materials because the synthesis is easy, inexpensive and suitable for large-scale production. The resulting high-surface-area materials and uniform pores promise to be suitable for use as absorbents, catalyst supports and materials for advanced electronic applications.

The main reason for undertaking this study was to produce a high surface area mesoporous carbon support. The secondary reason was to deposit Pt on the support using a suitable chemical deposition method. According to the literature, this can be achieved but the procedures for producing these materials are not well described by Su et al., (2005). In this study SBA-15 silica template was synthesized and sucrose was used as a source of carbon to produce the desired high surface area mesoporous carbon via a CVD method. A novel chemical vapour deposition method was used to deposit platinum nanoparticles on the OMC under high temperature and pressure. Therefore this study was to determine which variables were of importance and what conditions would be needed to produce a a high surface area mesoporous carbon with Pt supported on it.

CHAPTER 3

SYNTHESIS OF NANOPHASE SUPPORTS AND PLATINIUM ELECTROCATALYSTS

3.1 INTRODUCTION

The main objective of this chapter is to present the methods used for the preparation and comprehensive characterization of nanophase electrocatalysts. The chapter starts with the introduction of detailed methodology used for the preparation of nanophase. These materials were used as a support for the electrocatalysts described in the study. This is followed by a detailed literature review and listing of characterization techniques used in the study. Sample preparations and experimental parameters that were used in the investigation are also described.

This section will highlight materials and methods used for the fabrication and characterization of graphitisable and graphitised porous carbons with a well-developed mesoporosity. The synthetic route used to prepare the graphitisable carbons were: (a) the infiltration of the porosity of mesoporous silica with a carbon precursor (i.e. sucrose), (b) the carbonisation of the silica – sucrose composite and (c) the removal of the silica skeleton.

3.2 EXPERIMENTAL PROCEDURE

3.2.1 CHEMICALS

The chemicals that were used in the study are presented in Table 3.1

Table 3.1: Summary of chemicals used in the study

Chemical Name	Purity	Supplier
Tetraethoxysilane; TEOS	98%	Aldrich
Poly(ethylene oxide)-block-poly(propylene oxide)-blockpoly (ethylene oxide) triblock copolymer ($EO_{20}PO_{70}EO_{20}$), Pluronic P123	PEG, 30 wt. %	Aldrich
Ethanol	99.9%,	Kimix
Sodium hydroxide pellets	CP	Kimix
LPG	A mixture of propane and butane	AFROX
hydrochloric acid	37%	Aldrich
Sulphuric Acid	99%	Aldrich
Nitrogen Gas	Technical grade	AFROX
Commercial JM Pt/C catalyst	40% wt Pt, 4.2 nm particles	Johnson Matthey
Platinum (II) acetylacetonate, ($Pt(acac)_2$)	97%	Aldrich
Sucrose	99.5%, GC	Aldrich

3.2.2 SYNTHESIS OF SBA – 15

SBA–15 templates were prepared by a room temperature method (Piotr *et al.,* 2005). In a typical synthesis, 4.10 g of poly (ethylene oxide)-*block*-poly (propylene oxide)-*block*-poly-(ethylene oxide) tri copolymer ($EO_{20}PO_{70}EO_{20}$, Pluronic P123) was transferred to a 500 ml beaker. HCl (150 ml of 1.6 M) was added and the solution was left to stir for 30minutes. TEOS (9.14 ml) was added to the mixture dropwise at 3.55 ml/min (32.5min for every 1 ml of TEOS). The obtained suspension was stirred at 45 ^{o}C for 8 h and then aged at 80 ^{o}C for 15 h. The solid product was filtered, washed with distilled water and dried at room temperature for 1 hour. The solid product was heated in a furnace in air to 550 ^{o}C at a heating rate of 1 ^{o}C/min at then calcined at 550 ^{o}C for 8 hrs. (Scheme 3.1)

3.2.3 SYNTHESIS OF OMC USING SBA-15 AS TEMPLATE AND LPG AS CARBON SOURCE

The calcined and thus detemplated SBA-15 was used as a solid template for the preparation of mesoporous carbon material by a CVD method (Godogwana MSc thesis, 2006). In a typical synthesis 2.0 g of SBA-15 silica template was transferred to a ceramic boat and placed in a flow through quartz tube furnace. The furnace was heated to the target temperature of 800 ^{o}C from 50 ^{o}C at a heating rate of 2 ^{o}C/min under LPG flow as indicated in Figure 3.1. When the target temperature of 800 ^{o}C was reached, the LPG was sustained at this temperature for 90 min. Thereafter the LPG flow was stopped and the sample was taken out of the tube furnace to cool at room temperature. The resulting mesoporous silica/carbon composite was refluxed with 50 ml of 1M NaOH at 75 ^{o}C under stirring for 2 h to dissolve and remove the silica template as shown in Figure 3.2. Thereafter the solution was filtered with a 0.45 μm filter paper using a Buchner funnel. Finally it was washed with ultra pure water (3x100 ml) and then dried in air at 100 ^{o}C (Scheme 3.1).

3.2.4 SYNTHESIS OF ORDERED MESOPOROUS CARBON USING SBA–15 AS TEMPLATE AND SUCROSE AS CARBON SOURCE

OMC was prepared by an impregnation process following the method of Su *et al.* (2010). In a typical synthesis, 1.0 g of SBA–15, 1.25 g of sucrose, and 0.14 g H_2SO_4 were added to 5.0 g of ultra pure water (room temperature), and the resulting mixture was dried overnight at 80 ^oC. Thereafter, the solid product was grounded and heated to 160 ^oC for 4 h. After this, 0.8 g of sucrose, 0.09 g of H_2SO_4 in 2.0 g of ultra pure water and 1.0 g ethanol were added to the solid product which was then dried at 80 ^oC for 4 hrs and 160 ^oC overnight. Finally, the resulting solid product was carbonized from 50 to 900 ^oC at 2 ^oC/min and held at this temperature for a further 5 h under N_2 flow. The silica template was removed by using 1M NaOH (4 g NaOH/100 ml H_2O) under reflux for 2 h. Thereafter the solution was filtered with a 0.45 μm filter paper using a Buchner funnel and then it was washed with ultra pure water (3x100 ml) which was followed by drying in air at 150 ^oC for 5 h to yield a carbon sample (scheme 3.1).

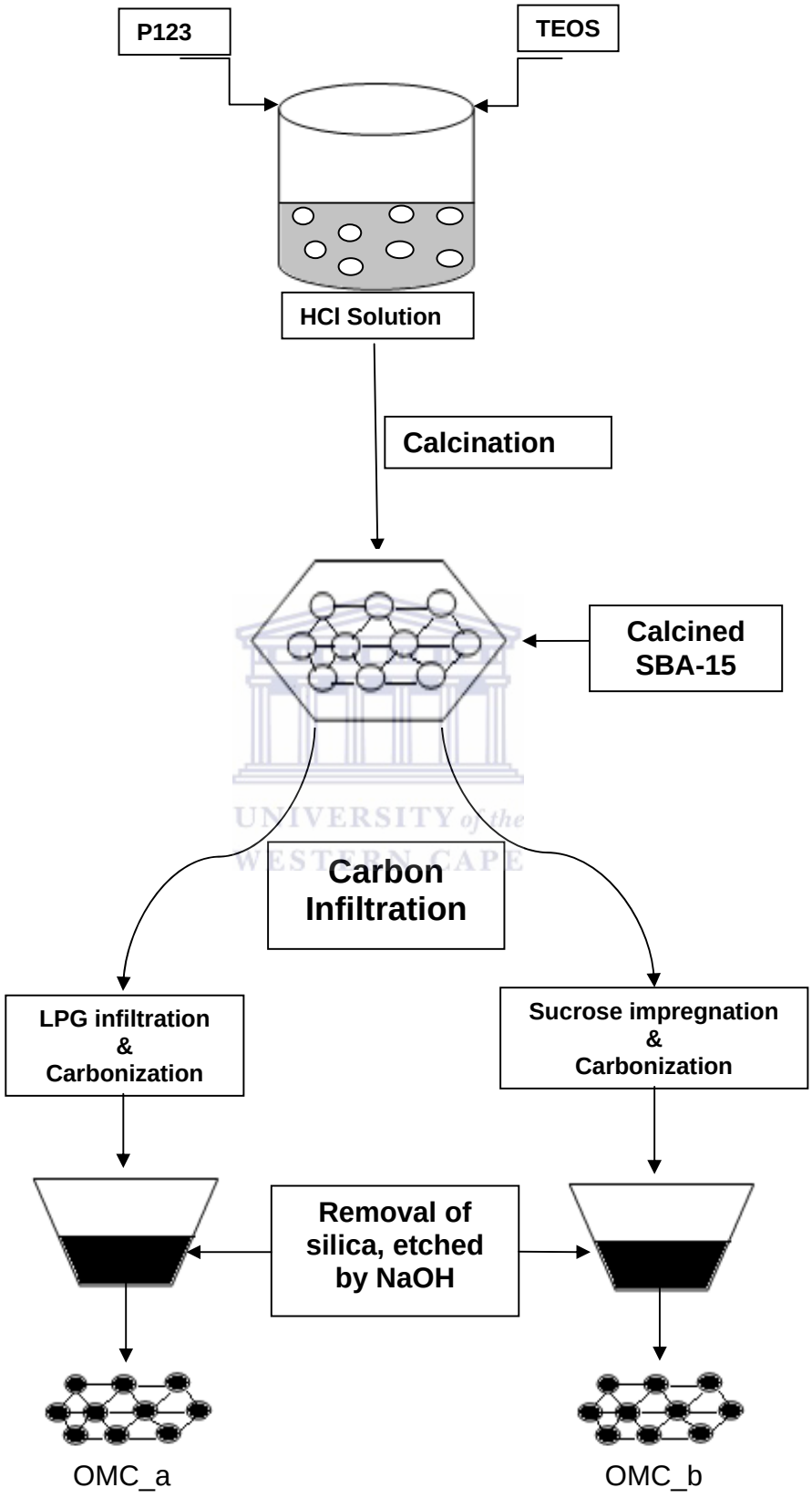

Scheme 3.1: Conceptual diagram for experimental design

3.2.5 CARBONIZATION OF EQUIPMENT

The set up for the carbonization of the silica/ carbon composite at high temperatures is illustrated in Fig 3.1 below. The carbonization was accomplished by placing a known quantity of a silica/carbon material in a ceramic boat followed by a flow of nitrogen gas.

Figure 3.1: Tube furnace for synthesis of carbon composites

The set up for the removal of the silica template is shown in Fig 3.2 below. This is achieved by refluxing a known quantity of silica/carbon composite with 1M NaOH.

Figure 3.2: Rotating heating mantle and round bottom flask with a thermometer

3.3 PREPARATION OF CATALYST

3.3.1 CHEMICAL VAPOUR DEPOSITION OF PLATINIUM ON MESOPOROUS CARBON

Platinum acetylacetonate, [$Pt(acac)_2$)], was physically mixed with a mesoporous carbon support in a mortar and pestle in order to grind and crush and mix the solid materials. This mixture was loaded into a reactor tube (diameter of 1cm, and length of 30cm). The reactor tube was firstly evacuated for 1 h to a pressure of 7.7 x 10^{-1} mbar. The tube was then slowly ramped to 100 °C and kept for another 1 hour to remove the trace of water. The pressure decreased substantially to 2.8 x 10^{-1} mbar. After sublimation of the platinum precursor, the tube was heated to 400 °C and held for 30 min to decompose the platinum precursor properly. The reactor tube was cooled to room temperature, and the sample was removed as reported by Suttisawat *et al.* (2009). The catalysts were synthesized using different amounts of the support and the precursor as shown in Table 3.2.

Table 3.2: % loading of Pt supported on OMC

Catalyst (% Pt)	OMC (g)	$Pt(acac)_2$ (g)
10	0.5	0.12
20	0.5	0.26
30	0.5	0.43

3.4 STRUCTURAL CHARACTERISATION OF NANOPHASE ELECTROCATALYST

The characterisation of nanomaterials plays a significant role both to prior and after evaluation of a catalyst since it is important to know the physical and the electrochemical characteristics of a catalyst. This information obtained on a catalyst prior to use helps with a better understanding of a catalysts abilities and also aids in the improvement of the activity of a catalyst. The catalyst surface is the physical property that allows the determination of the extent of absorption and desorption of the reactants and products respectively. The activity of a catalyst is directly proportional to the surface area to which the reacting species is exposed. The shape and size of the particles in a bulk catalyst does influence the activity of a catalyst, hence it is essential to have this information when developing an electrocatalyst. Sample characterisation techniques that were employed in this study are shown in Table 3.3:

Table 3.3: Characterization Procedures used during catalyst development

Type	Purpose
Fourier Transform Infra-Red (FTIR) Spectroscopy	Structural configuration and to assess the features of the amorphous silica
High resolution scanning electron microscopy & energy dispersive X–ray spectroscopy (HRSEM/EDS)	Morphology and qualitative elemental composition
High resolution transmission electron microscopy (HRTEM)/EDS	Crystallinity and particle size
X–ray diffractometer (XRD)	Crystallinity and particle size
Brunnauer-Emmet-Teller (BET) analysis	Surface area and pore diameter
Thermogravimetric analysis (TGA)	Determination of volatile species
Cyclic voltammetry (CV)	Electrochemical activity

3.4.1 FOURIER TRANSFORM INFRA-RED SPECTROSCOPY

3.4.1.1 EXPERIMENTAL DETAILS: SAMPLE PREPARATION

A 10 to 15 mg of sample was subjected to FTIR analysis. The sample was placed directly onto the FTIR probe. The probe was rotated into the sample which was situated on the sample holder.. The experimental conditions are given in Table 3.3.

Table 3.4: FTIR experimental instrument conditions

Instrument Name	Perkin Elmer spectrum 100 series FT-IR Spectrometer
Range	0 to 2000 cm^{-1}
Scan number	4
Units	Absorbance

3.4.2 X RAY DIFFRACTION

3.4.2.1 EXPERIMENTAL DETAILS: SAMPLE PREPARATION

The powder material was mounted on a sample holder; levelled using a spatula and finally it was introduced into the X–ray diffraction instrument. The instrument specification is listed in Table 3.4.

Table 3.5: The Siemens D8 Advance XRD operational parameters.

Parameter	Conditions
X – ray detector	Copper tube with Cu-Kα
Generator Voltage	40 kV
Generator Current	40 mA
Scanning Range	(0^o – 10^o) and (10^o – 90^o) (2θ angle)
Scan type	Locked coupled
Scan speed	60 s/step
Scan time	6 hrs
Step size	0.2^o
Wavelength	1.54 Å
Synchronous rotation	No

3.4.3 HIGH RESOLUTION SCANNING ELECTRON MICROSCOPY (SEM) / ENERGY DISPERSIVE SPECTROSCOPY (EDS)

The nanophase materials of interest were supported on double-sided conductive carbon tape and mounted on a sample stub. No sputter-coating was required as all the nanophase material used in the study were electron-conductive.

Samples were fitted into the vacuum chamber of the microscope (HRSEM, Zeiss Ultra 55 Field Emission – In-lens detection). High Resolution Scanning Electron Microscopy was used to probe the surface micro and macro structure, and determine the degree of agglomeration. Energy-dispersive X-ray spectroscopy (EDS) with a Hitachi X–650 SEM was used for elemental analysis and for chemical characterization of samples. Parameters for the HRSEM analysis are given below:

3.4.3.1 EXPERIMENTAL DETAILS: SAMPLE PREPARATION

A 15 mg sample was placed in a specially designed sample holder and this was mounted into the HRSEM instrument. The HRSEM instrument also had an attached EDS instrument connected to the computer for elemental analysis. The experimental conditions are listed in Table 3.5.

Table 3.6: HRSEM instrument experimental conditions

Parameter	Setting
Accelerating Voltage	30 kV
Current	10 nA
Emmiter	Thermal Field emision type
Aperture	0.4 mm
Resolution	1 nm
Standard detector	ESB with filtering grid
Magnification	900 K

3.4.4 HIGH RESOLUTION TRANSMISSION ELECTRON MICROSCOPY (HRTEM)

3.4.4.1 EXPERIMENTAL DETAILS: SAMPLE PREPARATION

HRTEM samples were prepared by dispersion of a spatula-tip of the catalyst of interest in 5 ml methanol solution, followed by sonication of the suspension. One drop of the suspension was deposited onto carbon holey grids and allowed to dry for 15 minutes. The methanol was allowed to evaporate at room temperature. Samples were mounted in a sample holder that was introduced into the shaft of the electron microscope. The experimental conditions are listed in Table 3.7.

Table 3.7: HRTEM instrument experimental conditions

Name of Instrument	**Tecnai G2 F20 X-Twin Mat FEGTEM**
High tension	200 KV
Extraction Voltage	3950 V
FEG emission current	54 uA
Condenser Aperture	3 mm
Objective aperture	2 mm
Gunlens	1 nm
Spotsize	3 nm
Imaging was with TIA CCD camera.	

3.4.5 BRUNAUER–EMMET–TELLER (BET) N2 ADSORPTION

3.4.5.1 EXPERIMENTAL DETAILS: SAMPLE PREPARATION

The surface area, pore volume and pore size distribution of samples were determined by means of the Brunnaer–Emmet–Teller (N_2 BET) technique using a Micrometrics Accelerated SA and Porosimetry (ASAP) 2010 system. Approximately 100 mg of the sample was transferred into a sample tube.

Samples were degassed and dried at 90 ^{o}C for 2 hrs and at 200 ^{o}C overnight under nitrogen gas in order to remove moisture and to free the pores of any impurities. The experiment was conducted isothermally at – 196 ^{o}C with a constant N_2 flow applied during the analysis.

3.4.6 THERMO – GRAVIMETRIC ANALYSIS (TGA)

The sample was placed on a microbalance (20 mg) in a controlled atmosphere chamber. This chamber has a heating system that could be programmed to heat the sample at predefined heating rate, and to associate a temperature with the mass measured by the microbalance. Results are reported in curves that show the sample weight loss as a function of the temperature. TGA measurements could be performed in nitrogen atmosphere, air or other gas flux, depending on the type of thermal properties under investigation.

3.4.6.1 EXPERIMENTAL DETAILS: SAMPLE PREPARATION

Each sample was loaded into an aluminium pan. The experiment was performed under a flow of nitrogen, whilst subjecting the sample to heating at a controlled rate. The experimental conditions are given in Table 3.7.

Table 3.8: TGA instrument experimental conditions

Name of Instrument	**TA instruments Q500 TGA**
Heating Range	25 ^{o}C - 1000 ^{o}C
Heating rate	10 ^{o}C/min
N_2 supply rate	50 ml/min

3.4.7 ELECTROCHEMICAL CHARACTERISATION USING CYCLIC VOLTAMMETRY (CV)

3.4.7.1 EXPERIMENTAL DETAILS: SAMPLE PREPARATION

The electrochemical performance of the chemically modified carbon materials was analyzed using a three-electrode configuration in aqueous 0.5 M H_2SO_4 electrolyte. Cyclic voltammetry was performed on a computer connected to a BAS/50W integrated automated electrochemical workstation (Bioanalytical systems, Lafayette, IN, USA). A conventional three electrode cell was used with an Ag/AgCl electrode as a reference, a platinum wire, a counter electrode and a bare modified electrode (electrocatalyst) as working electrode. The paste was prepared by hand mixing graphite and mineral oil in a 70:30 (w/w) ratio in an agate mortar until a homogenous paste was obtained. Thereafter the catalyst was added to an aliquot of the paste in a 1:10 (w/w) ratio and thoroughly blended together by grinding in an agate mortar and pestle. The paste was tightly packed into a PVC tube (2 mm internal diameter) and the electrical contact was provided by a copper wire connected to the end of the tube. The electrochemical experimental parameters are given in table 3.8.

Table 3.9: Electrochemical experimental parameters are given as follows:

Parameter	**Specification**
Electrolyte	0.5 M Sulphuric acid to cell. Degassed with nitrogen by saturation
Methanol	Added 3.2 ml Methanol to 100 ml Sulphuric acid
Working Electrode	Catalyst Paste (See Working Electrode preparation)
Counter Electrode	Platinum Wire
Reference Electrode	Ag/AgCl
Scan Rate	50 mV Base run (0.5 M H_2SO_4)
Scan range	Scanning range: -0.2 to 1.0 V

3.4.7.2 EXPERIMENTAL SET – UP

The experimental set up used in the electrochemical characterization of the Pt/C electrocatalyst using CV is displayed in Figure 3.3 together with the three electrode system used for investigations.

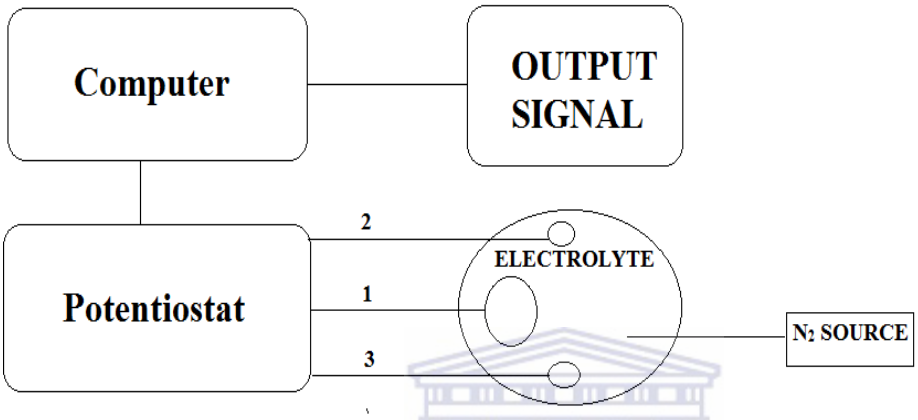

Figure 3.3: Experimental Set up for the electrochemical characterization

1. Working electrode; 2. Reference electrode; 3. Counter electrode

3.5 SYNOPSIS OF CHARACTERISATION METHODS

Characterization studies were determined by the structural properties that needed to be evaluated using characterization techniques, such as high resolution transmission and scanning electron microscopy as well as X-ray diffraction. The structural and chemical information and the characterization techniques used in their determination can be summarized as follows:

- Crystal structure, crystallinity and particle size of the material could qualitatively be examined by using XRD
- Surface morphology and length of mesoporous materials could qualitatively be examined using HRSEM
- Particle size and particle distribution could be examined by using HRTEM

- Total surface area and porosity of composite materials could qualitatively be examined by N_2 BET physisorption.
- Thermal stability of composite materials could quantitatively be examined by TGA.
- Electrochemical activity was determined using cyclic voltammetry.

CHAPTER 4

CHARACTERIZATION AND PHSYIOCHEMICAL ANALYSIS OF MESOPOROUS CARBON SUPPORTED PLATINUM

4.1 INTRODUCTION

This chapter presents and analyses the results obtained in this study. The findings are discussed in relation to the research questions. The structure of the chapter is aligned to the experimental methodology.

This study was undertaken to investigate if a mesoporous Si substrate SBA-15 would produce a high surface area mesoporous carbon support for high platinum dispersion. In this study the mesoporous Si support material, SBA-15 was used as a template to form a SBA-15 carbon composite and the carbon analogue of SBA-15. In Section 4.2, the substrate preparation is explained. In Section 4.3, mesoporous silica characterization results are illustrated and in Section 4.4, the characterization results of mesoporous carbon are described. In Section 4.5 the electrocatalytic behaviour of platinum on carbon is elucidated.

This SBA-15 was chosen as a sacrificial template for carbon deposition because it is reported to be a high surface area mesoporous carbon. The experimental approach of preparing this template is found in section 3.2.3 and the characterization of this material is shown in section 4.2.

4.2 CHARACTERIZATION OF MESOPOROUS SILICA (SBA-15)

Mesoporous silica SBA-15 was synthesized, as reported by Piotr et al. (2005) in a cooperative self-assembly process under acidic conditions using the triblock copolymer Pluronic 123 ($EO_{20}PO_{70}EO_{20}$) as template and tetraethoxysilane (TEOS) as the silica source (See section 3.2.3). The synthesis of SBA-15 was initiated by dispersing amphiphilic copolymer P123 in water and hydrochloric acid solution. Tetraethoxysilane (TEOS) was added to this solution as a source of silica. The solution was aged for 8 hours

at 80°C prior to filtering and washing. After synthesis, the organic pore filling template was removed by calcination (yield, ca. 100%).

This section will highlight the characterization results obtained for the mesoporous Si substrate (SBA-15) and the corresponding carbon analogue. The details of the characterization methodologies were outlined in section 3.2.3 and 3.2.5. The mesoporous silica (SBA-15) results are presented in the order: FTIR spectra, XRD data, BET data, EDS data, HRTEM and SEM images.

4.2.1 SBA-15 ANALYSIS BY FOURIER TRANSFORM INFRA-RED (FTIR) SPECTROSCOPY

The main reason for doing FTIR spectroscopy was to check if the template was fully removed from the carbon and to establish if the pores are clean. The FTIR spectra of SBA-15 Si template is shown in Figure 4.1.

In Figure 4.1(a), the FTIR spectra of the uncalcined and the calcined SBA-15 (2000 – 500cm^{-1}) are presented.

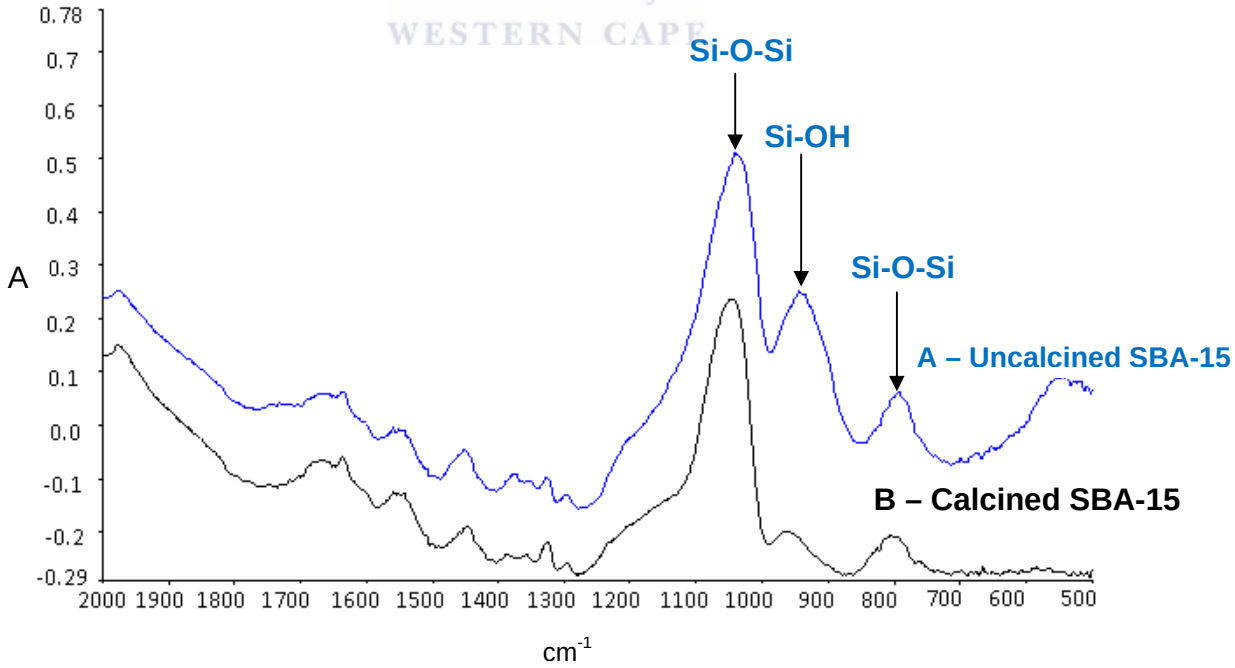

Figure 4.1(a): FTIR spectra of SBA-15 before (A) and after (B) calcination

The major bands occurring at 1070 cm^{-1} and 800 cm^{-1} for uncalcined SBA-15(A) were assigned to stretching vibrations of Si–O–Si (Innocenzi et al., (2003)). A band of medium intensity centred at 950 cm-1 is characteristic of Si-OH stretching vibrations (Innocenzi et al., (2003)). The ratio of the Si–O–Si and Si-OH for the uncalcined vs the calcined bands is different as shown in Table 4.1. This is an indication of the evolution of porosity as a result of the heat treatment as reported by Innocenzi et al., (2003) and Kokunešoski et al., (2010).

Table 4.1: FTIR Absorbance for uncalcined and the calcined SBA-15.

Absorbance	SBA-15(A)	SBA-15(B)
Si-O-Si	0.5, 0.08	0.2; -0.08
Si-OH	0.2	-0.2

In Figure 4.1(b), the FTIR spectra for the organic bands of the uncalcined and the calcined SBA-15 are presented.

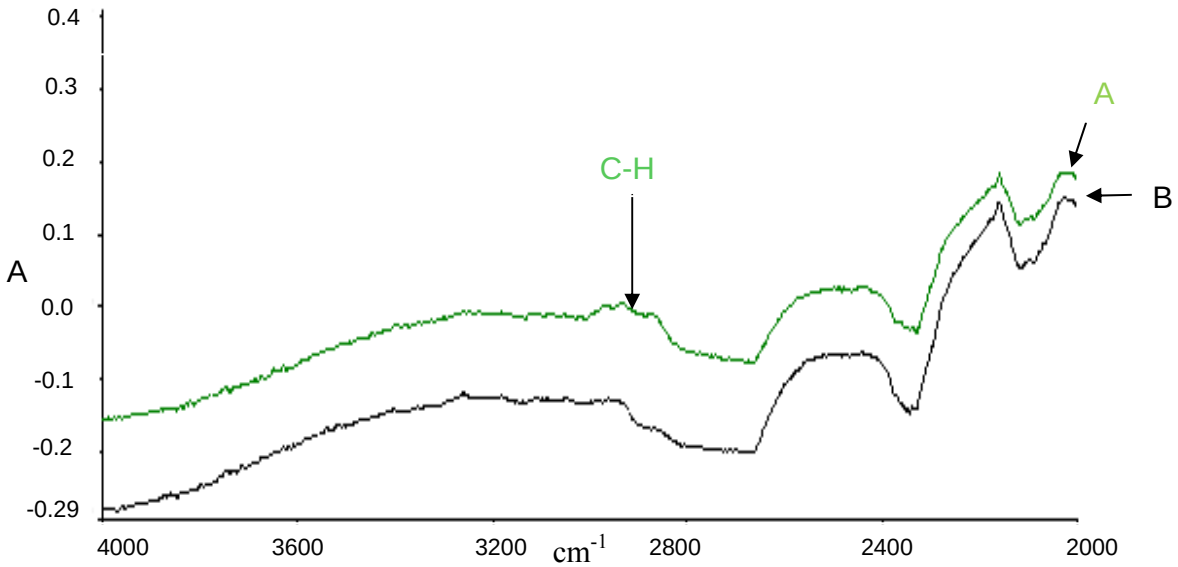

Figure 4.1(b): FTIR spectra of the organic bands of SBA-15 before (A) and after (B) calcination

The weak band appearing for the uncalcined SBA-15(A) between 2800 and 3000cm-1 is an indication of C-H stretching modes due to the template (Innocenzi et al., (2003)). These bands show a decrease in absorbance for the calcined SBA-15(B) indicating that the surfactant present in the uncalcined SBA-15 was removed (Innocenzi et al., (2003)).

4.2.2 SBA – 15 ANALYSES BY X – RAY DIFFRACTION (XRD)

The low angle XRD pattern of calcined mesoporous silica (SBA-15) is shown in Fig 4.2 and the wide angle XRD is given in Fig 4.3. The main reason for performing XRD was to verify the regular periodicity in SBA-15.

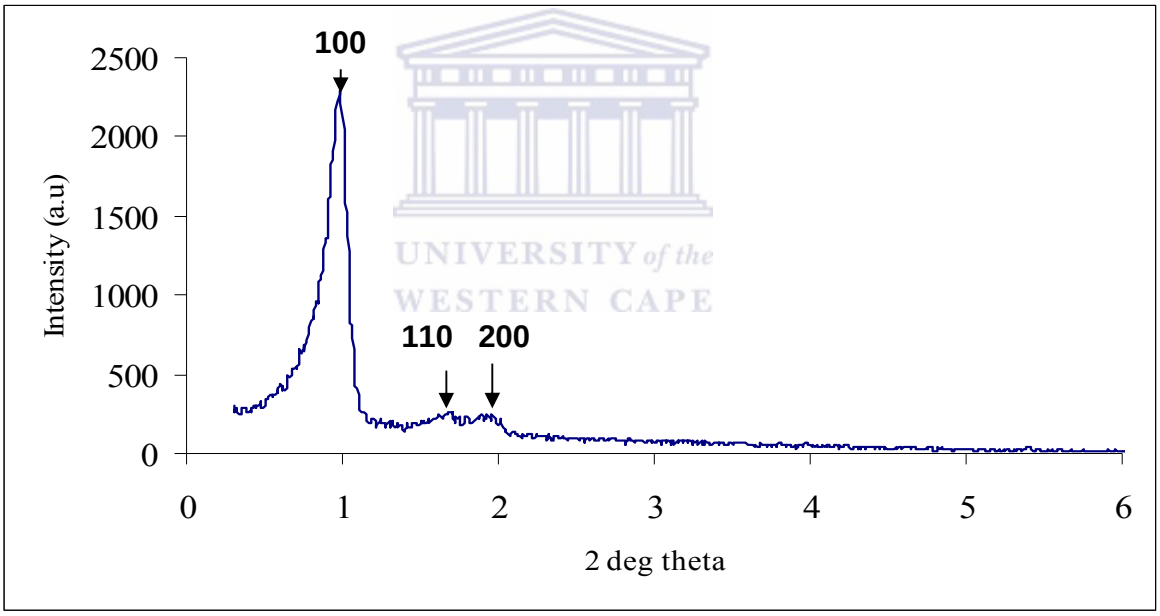

Figure 4.2: Low Angle XRD of SBA-15

The SBA–15 sample shows three resolved peaks at the small-angle XRD in the range of ~ 0.8–2^{o} 2θ that can be basically indexed as (100), (110), and (200) reflections associated with the 2-D hexagonal P6mm symmetry, indicating the ordered arrangement of the nanopores in SBA–15, in their highly ordered mesostructure (Zhai et al., (2008)). The d_{100} peak reflects a d spacing of 9.3 nm that correspond to the P123-directed hexagonal pore structure. Similar XRD reflections as indicated in Figure 4.2 with a d spacing of 9.2

nm which is comparable to SBA-15 in this study were reported by Zhai et al., (2008) and Jin et al., (2008).

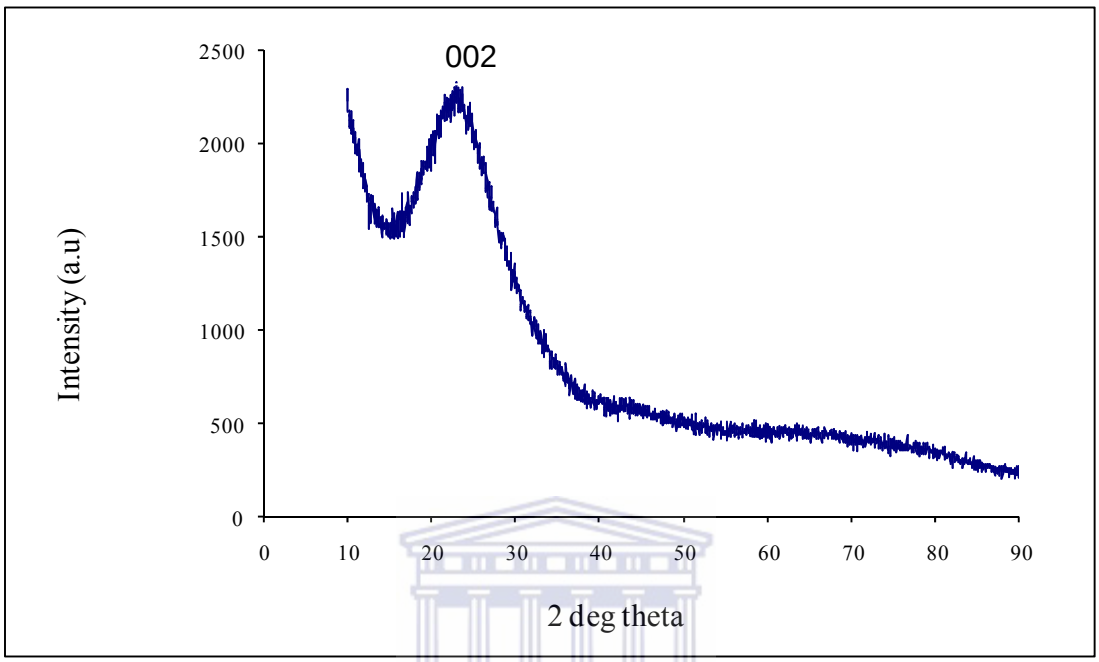

Figure 4.3: Wide Angle XRD of SBA-15

The wide angle XRD of SBA-15 shows the presence of a broad XRD peak at ~ 25^{o} 2θ, which is characteristic of amorphous silica (Du *et al., 2008)*

4.2.3 SBA – 15 ANALYSIS FROM NITROGEN ADSORPTION/ DESORPTION ISOTHERMS

N_2 BET adsorption/desorption was performed on SBA-15 at 77 K using a Micromeritics ASAP 2010 automatic analyzer in order to evaluate the pore size and surface area of the micropore and mesopore regions of the SBA-15.

The nitrogen adsorption/desorption and pore size distribution plots are shown in Figure 4.4 and Figure 4.5.

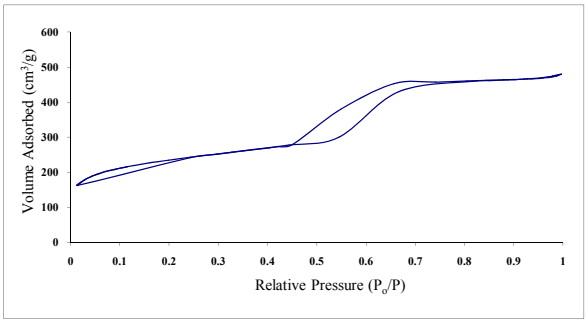

Figure 4.4: Adsorption/desorption isotherm for SBA-15 by BET method

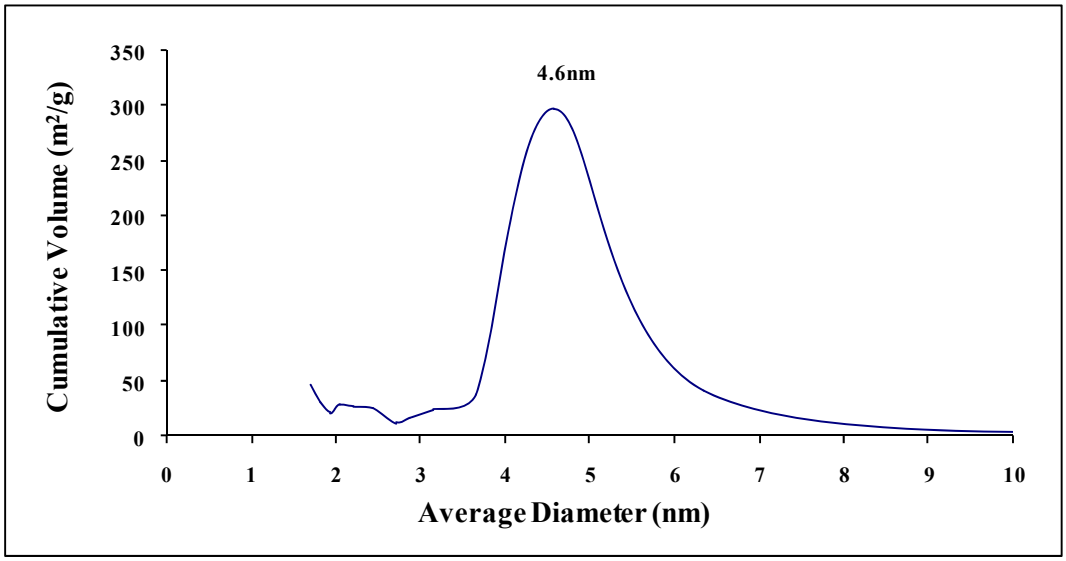

Figure 4.5: Pore size distribution for SBA-15 by BJH method.

Figure 4.4 and 4.5 shows nitrogen adsorption and desorption isotherm and the pore size of the synthesized mesoporous silica (SBA-15). The mesoporous silica material yielded a type IV isotherm with a type H1 hysteresis loop which suggests the material has regular mesochannels as confirmed by HRTEM with similar results reported by Zhao et al., (1998). There is a sharp inflection at relative pressure Po/P $\geq$ 0.4, characteristic of capillary condensation of nitrogen as explained by Joo *et al.,* (2008), which indicates the uniformity of the mesopore size distribution. The surface area of SBA-15 silica was found to be 854 m^2/g and a total pore volume of 0.62 cm^3/g.

The SBA-15 shows the presence of micropores in Figure 4.4. The micropore surface area of SBA-15 was 293 m^2/g. This was determined by the total surface area of SBA-15 and the incremental surface area for the mesopore region. Ryoo *et al.,* (2001) and Morishige *et al.,*(2004) attributed the existence of micropores to the microporous interconnections between the mesopores of SBA-15.

The corresponding pore size distribution data for SBA-15 silica template is shown in Figure 4.5 as calculated from the nitrogen isotherms adsorption branches by the Barrett–Joyner– Halenda (BJH) method. This showed that the pores were uniform with a narrow pore size distribution centred at 4.6 nm which confirms the results obtained by HRTEM for SBA-15. The approximate pore size calculated using the BJH analysis is significantly smaller than the pore size determined by XRD, using the Scherrer equation. This is because the latter includes the thickness of the pore wall. The thickness of the pore wall is estimated to be 3 nm for SBA-15 prepared with $EO_{20}PO_{70}EO_{20}$ as shown by Zhao et al., (1998). Zhao et al., (1998) reported a N_2 BET surface area of 850 m^2/g with a pore volume of 1.17 cm^3/g and a pore size of 8.9 nm which is similar to the findings for SBA-15 prepared in this study.

4.2.4 SBA-15 BY HRTEM

Figure 4.6 shows the HRTEM of SBA-15. The main reason for doing HRTEM analysis of SBA-15 is to observe the periodic arrangement of the pores.

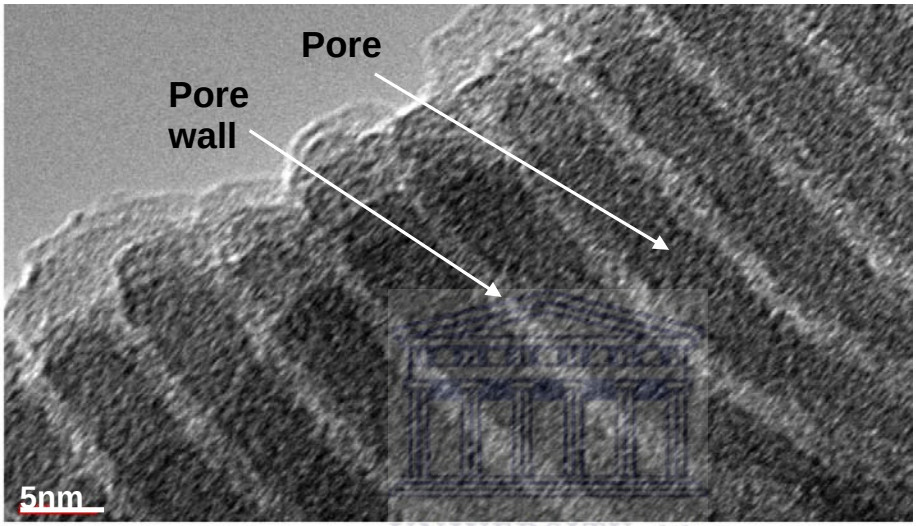

Figure 4.6: HRTEM image of SBA-15

From Fig. 4.6, it can be seen that the ordered pore arrangement of SBA-15 is retained and it shows the parallel mesochannels with dimensions of approximately 5 nm. This is further confirmed by the high surface area of SBA-15 and the BJH pore diameter of 4.6 nm. The HRTEM image confirms the ordered structure of the material, and shows the cylindrical pores are arranged in a well-ordered hexagonal array of mesopores. Similar results were reported by Zhao *et al.,* (1998).

4.2.5 SBA-15 MORPHOLOGY BY HRSEM

The main reason for performing HRSEM was to assess the morphology and particle size of the SBA-15. The characterization methodology is found in section 3.4.3.1. Figure 4.7 shows the HRSEM image of the SBA-15.

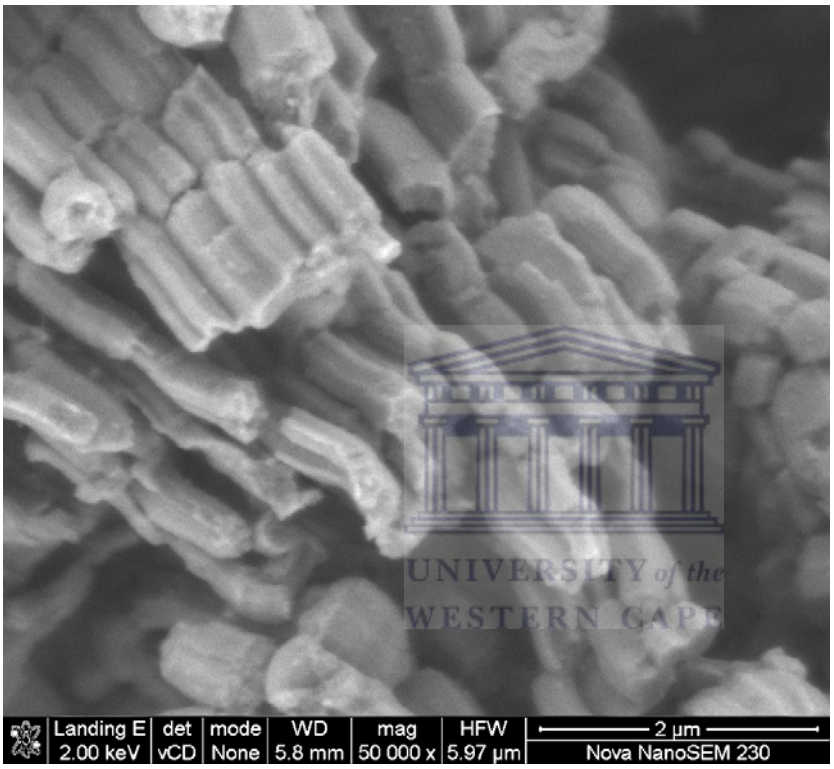

Figure 4.7: HRSEM image of SBA–15

In Figure 4.7 the particles are arranged with rod-like morphologies made up of bundles of parallel arranged channels with a diameter of 0.5 µm and with lengths of about 1-2 µm. The particles appear to be agglomerate. The HRSEM images reported by Katiyar et al. (2006) were similar in magnitude and morphology.

4.3 CHARACTERIZATION OF ORDERED MESOPOROUS CARBON (OMC)

Ordered mesoporous carbon was synthesized using two different methods with two different carbon sources: (a) LPG carbon source using a CVD method and, (b) sucrose infiltration followed by carbonization.

(a) LPG carbon source using a CVD method: In this method, the synthesis of OMC using LPG by depositing the carbon into pores of the SBA-15 silica template at high temperature using CVD technique was attempted. The weight increased after LPG impregnation. The temperature of the reaction was increased to 800^0C and held at this temperature for 90 minutes under LPG and thereafter allowed to cool to room temperature under nitrogen. The removal of SiO_2 by NaOH dissolution was not successful as the silica content was found to be approximately 25% by EDS analysis. In Figure 4.8 the XRD spectrum (see section 3.2.4) of OMC (*via* route a) is shown.

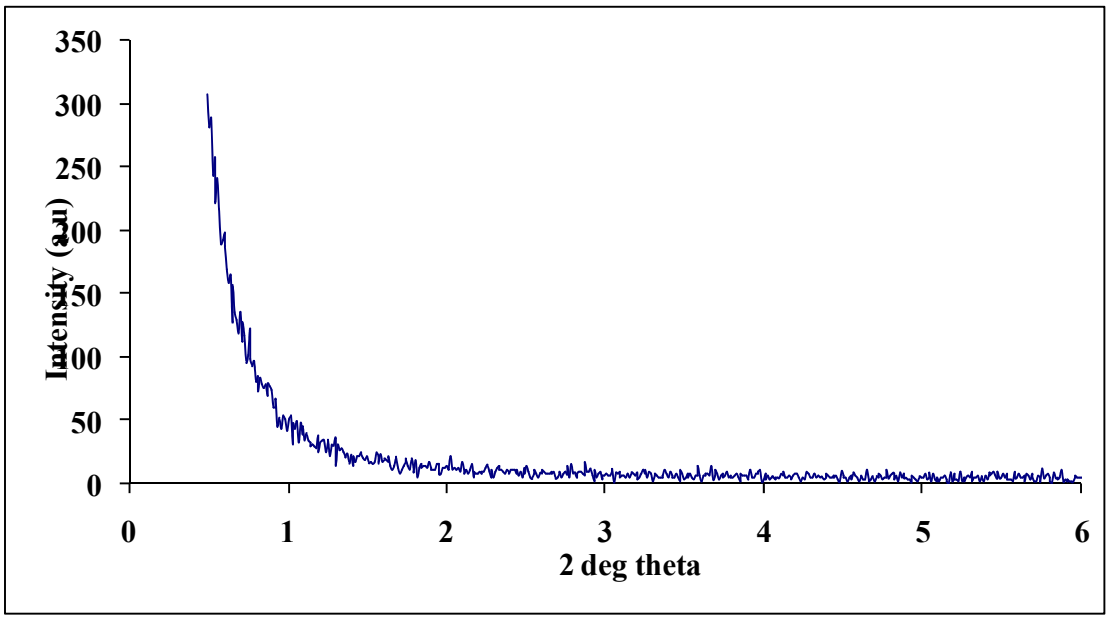

Figure 4.8: XRD for OMC (*via* route a)

In Figure 4.8, it is evident that no low angle peaks were retained in the carbon product after removal of the silica template.

The N_2 adsorption/desorption isotherm by BET of OMC is shown (*via* route a) is shown in Figure 4.9.

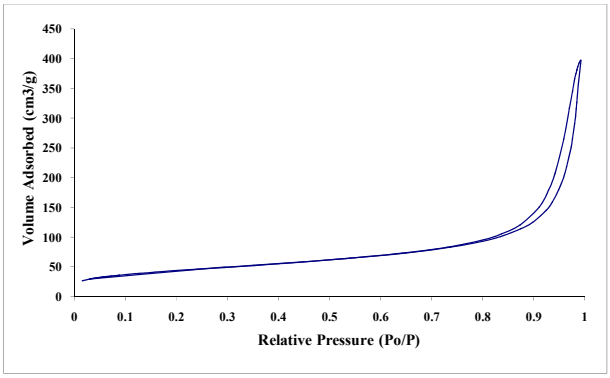

Figure 4.9: Adsorption/Desorption Isotherm for OMC (*via* route a) by BJH method

The OMC has a low microporosity as shown in Figure 4.9. The micropore surface area of OMC was 4.8 m^2/g and the external surface area was 149 m^2/g. Thus yielding a total surface area of 153.8 m^2/g.

In Figure 4.10, the pore size distribution of OMC (*via* route a) is shown.

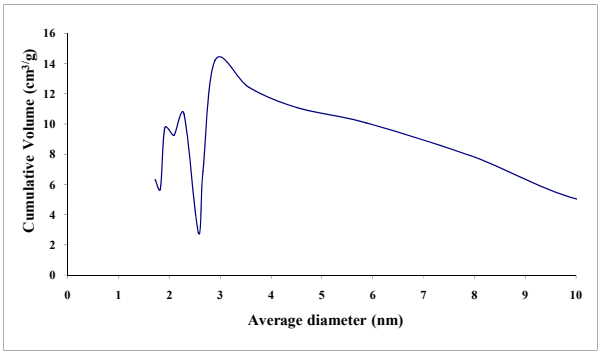

Figure 4.10: Pore size distribution for OMC (*via* route a) by BJH method

The low angle XRD showed in the nanometre region indicates the broad pore size distribution of OMC as shown in Figure 4.10, indicating a highly convoluted external surface.

The explanation of these results from OMC *via* route (a) can be described in scheme 4.1.

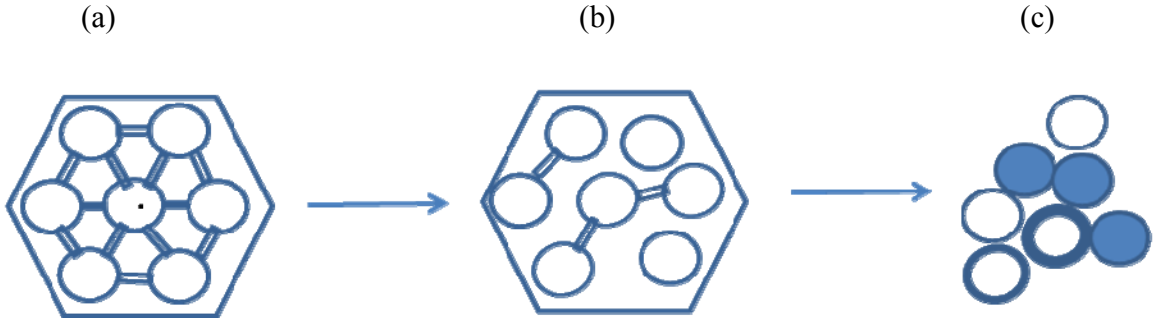

Scheme 4.1: Schematic diagram for attempted prepartion of OMC via LPG infiltration and carbonization method using SBA-15

The figure shows the mesostructure of SBA-15 on scheme 4.1(a). Addition of LPG covers whole SBA-15, not just hole. Finally, the removal of the silica template by NaOH resulted in a disordered OMC as confirmed by the absence of a low angle XRD peak (Figure 4.8) and the very low surface area of 153.8 (Figure 4.9). This could be due to the mesoporous framework of SBA-15 collapsing during the carbonization process at high temperature to produce amorphous structure (Scheme 4.1). The pore size distribution of OMC prepared using route A is shown in Figure 4.10 and clearly indicates that there are broad pores and a high external surface area. No further characterization was done on this OMC sample.

(b) Sucrose impregnation followed by carbonization: This method involved the impregnation of the pores of mesoporous silica, SBA-15, (refer to Section 3.2.4) with sucrose followed by carbonization at 800°C. Finally the silica template was removed by NaOH etching to obtain the desired high surface area mesoporous carbon as shown in Scheme 4.2.

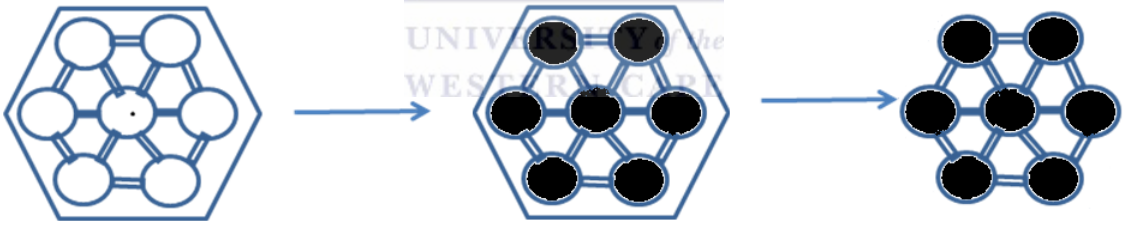

Scheme 4.2: Schematic diagram for prepartion of OMC via sucrose impregnation and carbonization method using SBA-15 (route b)

Characterization results of the synthesized ordered mesoporous carbon (OMC) are presented below using various techniques such as and FTIR spectroscopy, XRD, and TGA, HR-SEM and EDS.

4.3.1 FOURIER TRANSFORM INFRA–RED SPECTROSCOPY OF CARBON INFILTRATED SILICA TEMPLATE AND OMC (using route b)

The reason for performing FTIR analysis was to assess the presence of silica functional groups in the OMC prepared by route b. The detail of the methodology for performing FTIR is found in section 3.4.1.1. The characteristic Si bands in Figures 4.11(A) show a decrease in absorbance of Si-O-Si bands relative to Figures 4.11(B) as more carbon begins to fill the pores of the SBA-15. As expected no silica bands are present in Figure 4.11(B) which is the OMC obtained *via* route (b) thus indicating the complete removal of the silica template by NaOH dissolution.

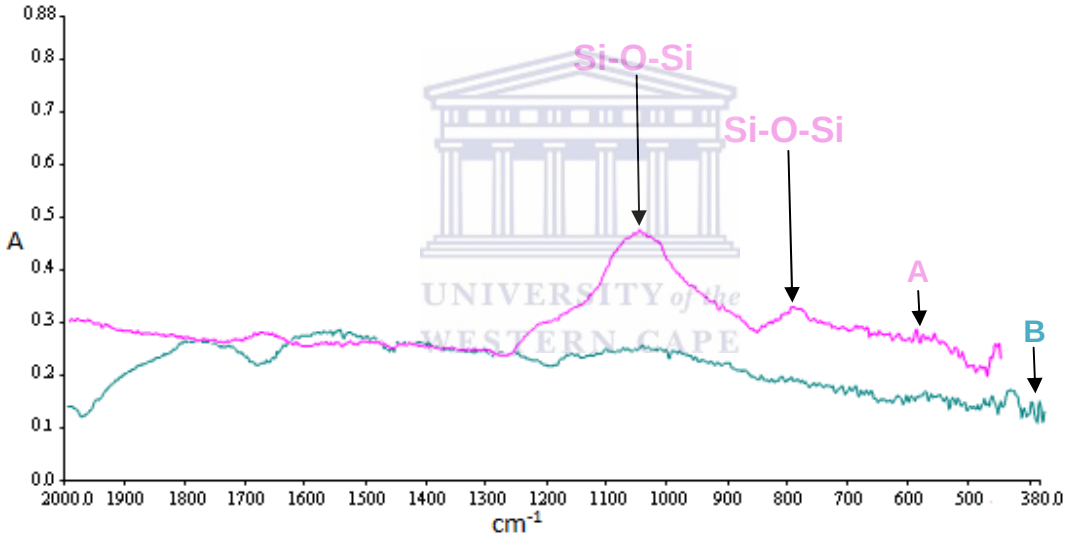

Figure 4.11: FT-IR of silica carbon template (A) and the OMC (B) (*via* route b)

4.3.2 X–RAY DIFFRACTION ANALYSIS OF OMC (using route b)

Figure 4.12 shows the low angle XRD pattern of the carbon product OMC (*via* route b).

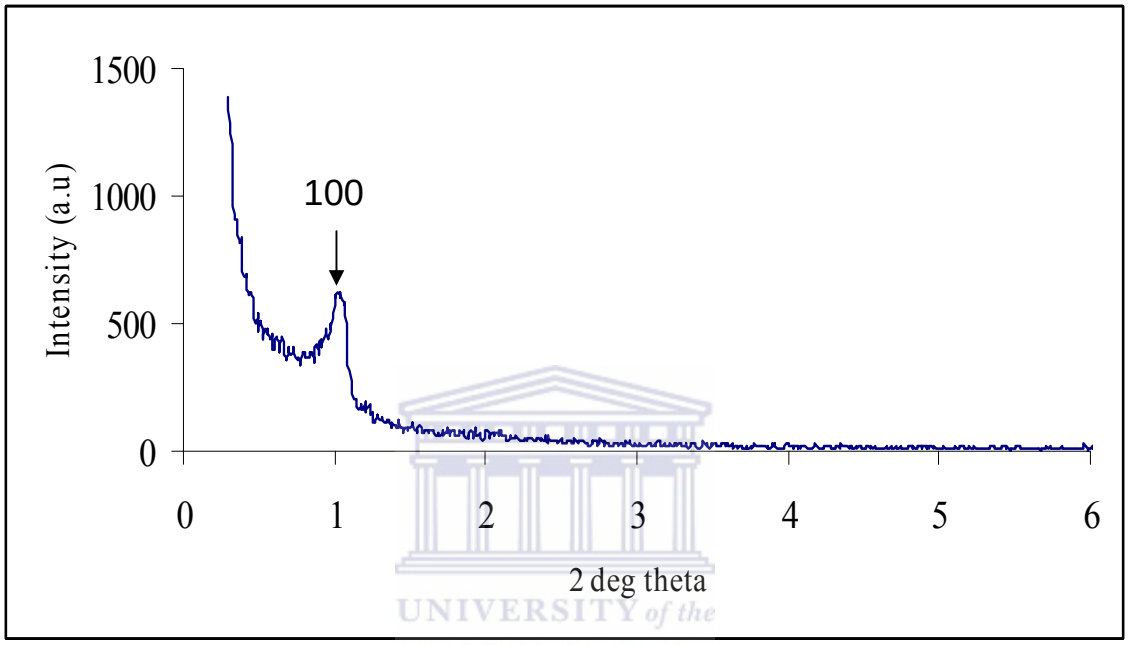

Figure 4.12: Low angle XRD of OMC (*via* route b)

In Figure 4.12, the peak observed can be assigned to the (100) diffraction of p6mm hexagonal symmetry. From the Bragg equation, the average pore size spacing is estimated to be 8.41 nm which is somewhat lower than that obtained from SBA-15. This observation is ascribed to the structure shrinkage of carbon materials during carbonization and the template removal process. The low angle XRD pattern (100) peak indicates the presence of uniformly sized pores for ordered materials as reported by Coville *et al.*, (2010).

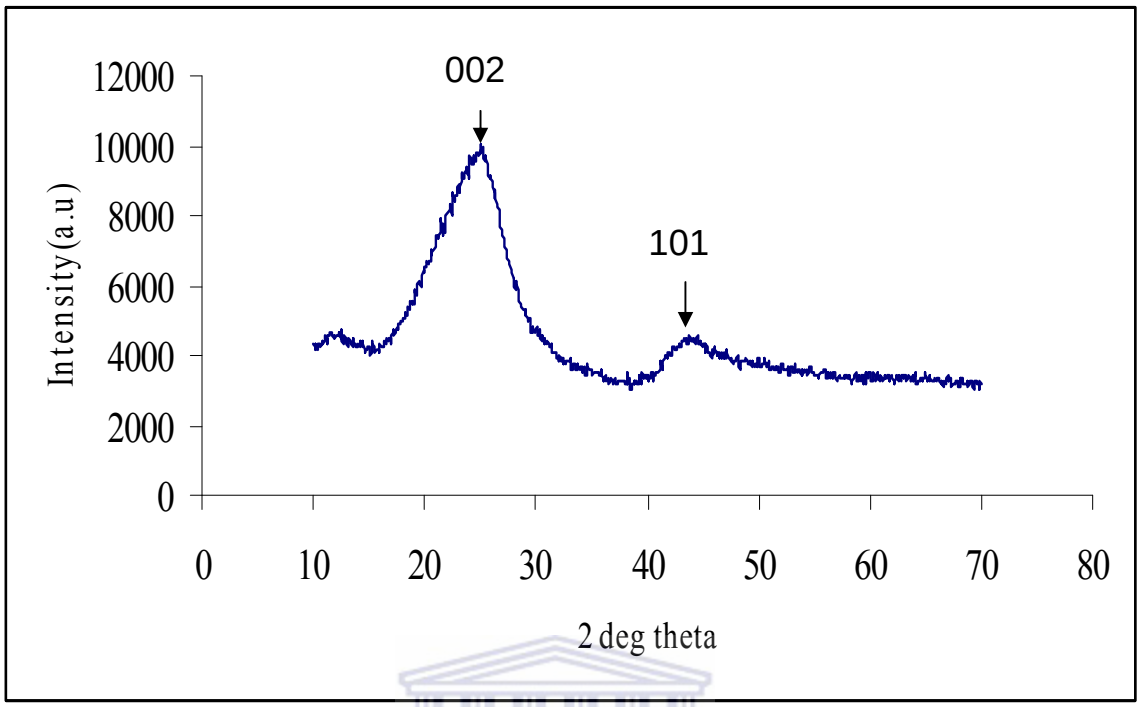

Figure 4.13: Wide angle XRD of OMC (*via* route b)

Figure 4.13 shows the presence of wide angle XRD patterns at ~ 24^{o} and 43.5° 2θ, which are the (002) and (101) from the graphitic carbon formed during carbonization at 800°C. This diffraction peak showing a reflection at ~ 25° corresponds to 0.36 nm graphite layer spacing. Similar observations were reported by Kruk et al., (2007). This is an indication that the pore walls of OMC derived from SBA-15 was ordered on the atomic scale although the carbon was similar to the graphitized structure (*d*002 = 0.343 nm) (Yang *et al.*, (2004)).

4.3.3 HIGH RESOLUTION SCANNING ELECTRON MICROSCOPY (HRSEM) OF OMC (via route b)

The main reason for performing HRSEM was to obtain information about the morphology and agglomeration of particles of the OMC structure. The experimental procedure for HRSEM of OMC (via route b) can be found in section 3.4.3.1.

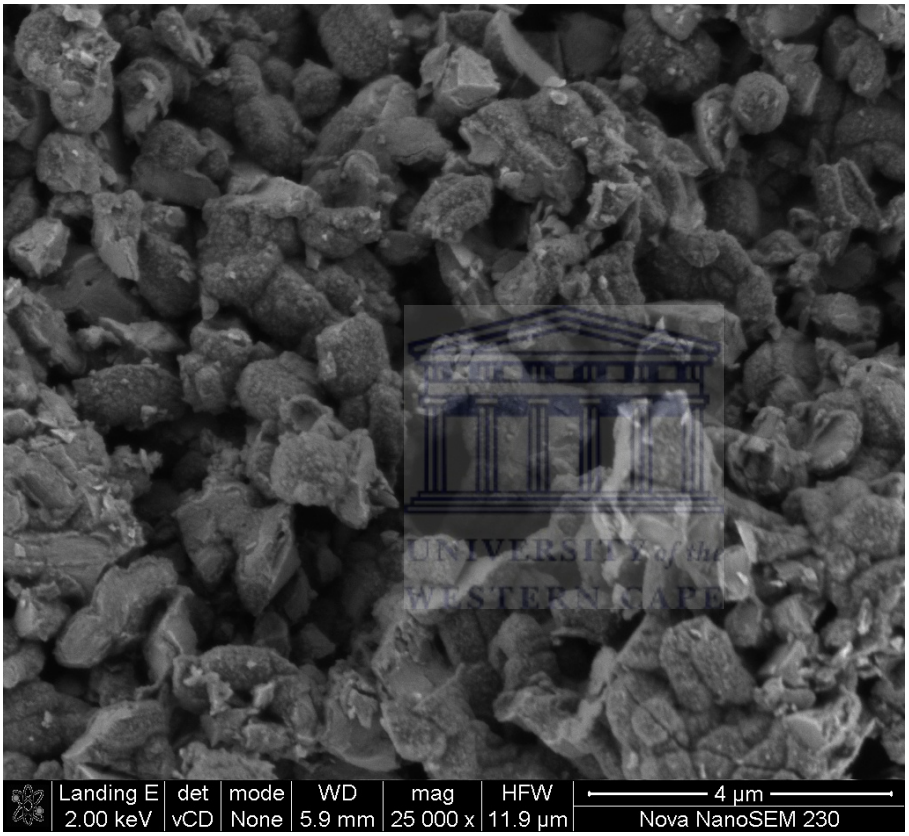

Figure 4.14: HRSEM of OMC (*via* route b)

Figure 4.14 reveals that the carbon particles are segregated, suggesting that no agglomeration of the carbon particles occurred during the CVD process. It is quite evident that the hexagonal morphology was not visible due to structural shrinkage as confirmed by XRD low angle analysis. Fang et al., (2010) observed a similar morphology in that the carbon particles were separated from one another.

4.3.4 SURFACE AREA AND PORE SIZE VOLUME ANALYSIS OF OMC PRODUCT (*via* route b)

The main reason for performing BET analysis was to evaluate the surface area and pores of the micropore and mesopore region of the OMC. The textural properties of the synthesized carbon support are given in table 4.1.

Table 4.2: Textural Properties of OMC (via route a and b)

Sample	S_{BET} (m^2/g)	V_t (cm^3/g)	ω_{BJH} (nm)
OMC (route a)	153	0.6	Diffuse (2-10 nm)
OMC (route b)	2115	0.60	2 – 4

* S_{BET} = BET surface area, V_t = Total pore volume, ω_{BJH} =Pore diameter derived from BJH

The surface area and pore size distribution OMC was obtained from the BET data and was close to that obtained in the literature that was found to be 2390 m^2/g (Li et al. (2007)).

In Figure 4.15, the nitrogen adsorption/desorption isotherm of OMC via route b is presented.

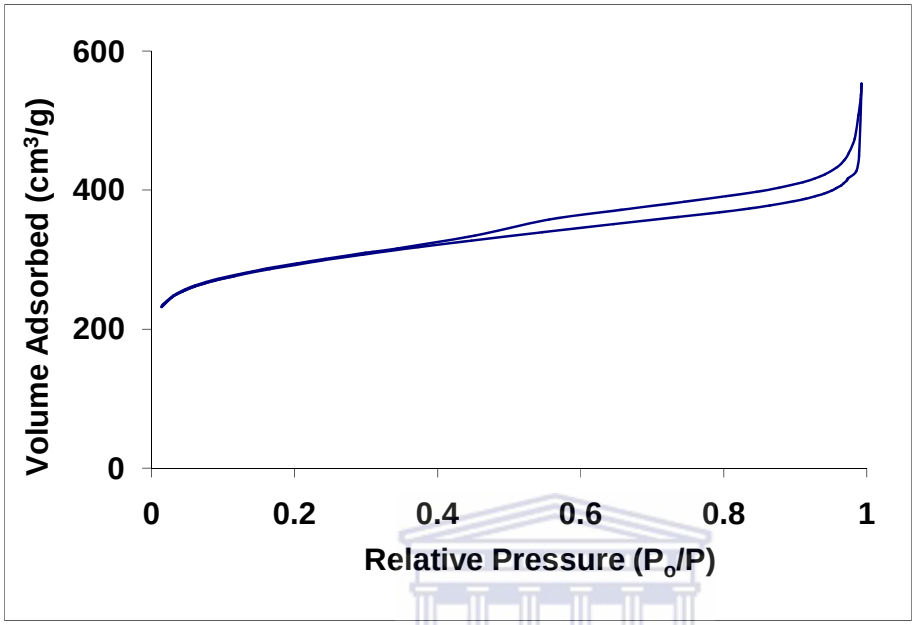

Figure 4.15: Adsorption/Desorption Isotherm for OMC (*via* route b)

It can be seen that the adsorption isotherm of OMC as shown in Figure 4.15 represents a with a type IV pore structure and a hysteresis loop of type 2 according to the International Union of Pure and Applied Chemistry (IUPAC) classification, indicative of a mesoporous material. The nitrogen uptake above the relative pressure of 0.40 is due to the capillary condensation of nitrogen in the mesopores.

The OMC (*via* route b) shows the presence of micropores in Figure 4.15. The micropore surface area of OMC (*via* route b) was 663.15 m^2/g. This was determined by subtracting the total surface area of OMC (*via* route b) from the incremental surface area for the mesopore region.

In Figure 4.16, the pore size distribution of OMC (*via* route b) is presented.

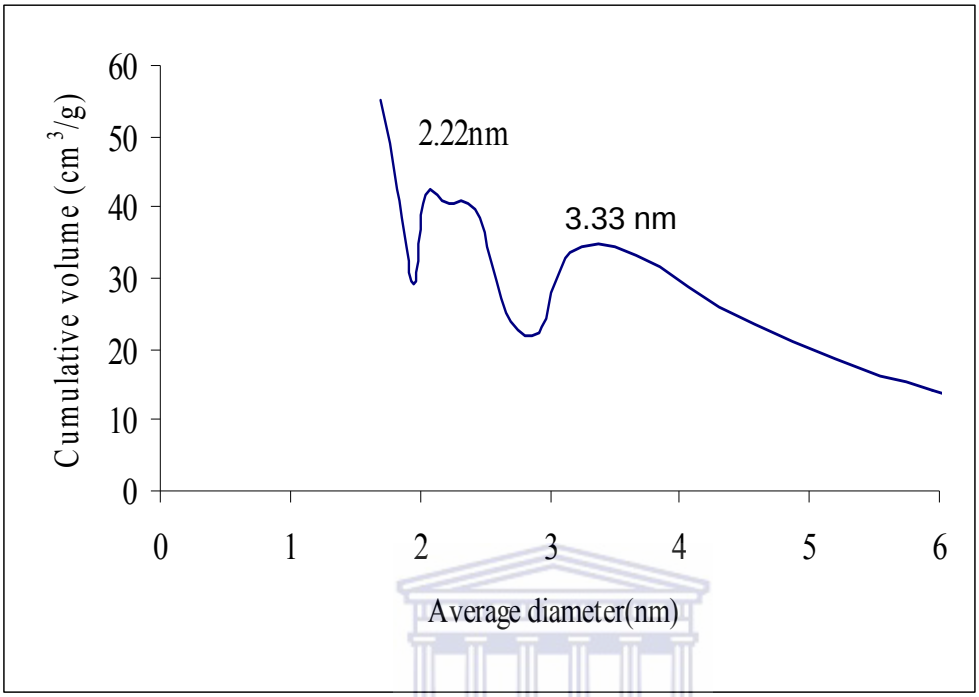

Figure 4.16: Pore size distribution (PSD) of OMC (*via* route b)

The PSD as shown in Figure 4.16 was derived from the BJH method and indicates a bimodal distribution of mesopores in the OMC with pore sizes of 2 – 4 nm respectively. The presence of these pores in the mesopore region indicates that the OMC possess a system of interconnected pores. It is known that SBA-15 mesoporous silica possess mesopores interconnected with micropores (Antolini, 2009).

4.3.5 ENERGY DISPERSIVE SPECTROSCOPY (EDS) ANALYSIS OF SBA-15 AND OMC

Energy Dispersive Spectroscopy (EDS) analysis was performed on SBA-15 and OMC (*via* route b) in order to determine the composition of the surface elements and data are given in Table 4.3. The average of 10 spots was taken for the EDS analysis. Thus, it can be seen from Table 4.3 that the content for SBA-15 includes only silica and oxygen atoms as expected from the SiO_2. In the case of OMC (*via* route b) the major element present is carbon atoms as expected, thus indicating the successful and near complete

(1.26 residue) removal of the silica template from the final OMC product. The EDX results represented in Table 4.2 complimented the TGA data and the FTIR data and clearly showed that more than 98 % of carbon is present in the OMC (*via* route b).

Table 4.3: Energy Dispersive Spectroscopy for SBA-15 and OMC (via route b)

Element	SBA- 15 (Mass %)	OMC (via route b) (Mass %)
Si	61±3	1.52
O	38±4	0.0
C	0	98.48

4.3.6 THERMOGRAVIMETRIC ANALYSIS OF OMC (*via* route b)

Thermogravimetric weight changes of OMC were recorded under a nitrogen atmosphere and were used to determine the carbon decomposition of the OMC. The corresponding results are presented in Fig. 4.17.

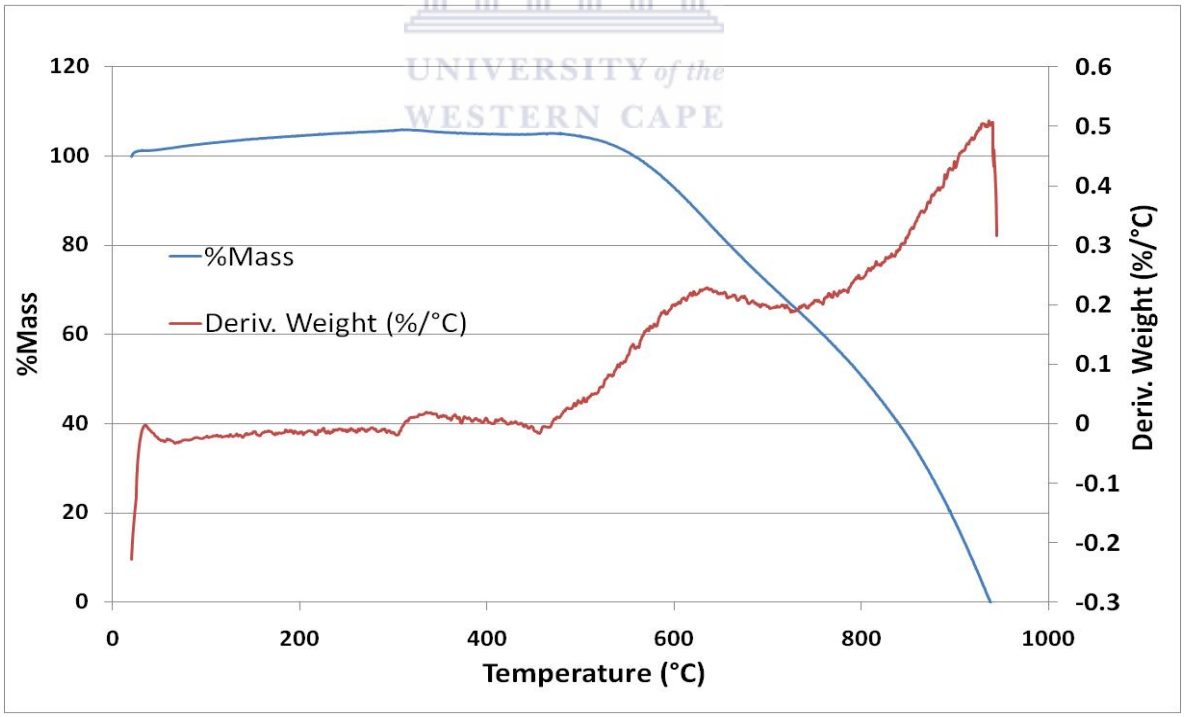

Figure 4.17: TGA and DTG of OMC

The possible reasons why there appears to be sample drift at temperatures around 100^{o}C is due the relatively small sample (few milligrams). The mass loss usually occurring in this region is related primarily to the thermo-desorption of physisorbed water.

In Figure 4.17, there appears to be no mass loss at T < 500 ^{o}C for mesoporous pyrolysed sample (silica template removed). The region beyond 500 ^{o}C shows that 30% of the carbon was combusted indicating that the partially graphitised more stable form of carbon constituted about 70 % of the carbon formed after a pyrolysis step at 900 ^{o}C. These results provide additional confirmation of the graphitized nature of the mesoporous carbon frameworks, which is responsible for the much improved thermal stability. It can be observed from DTG curves of the composite (Fig 4.17) that OMC (*via* route b) has two peaks centred at 640 and 915 ^{o}C, indicating regions of graphitic versus amorphous carbons region in the matrix. The most fundamental information from the TGA curve is that the silica template was almost completely removed (1.52% SiO_2 residue) by dissolution using NaOH because of the nearly zero residues at 940 ^{o}C, confirming that OMC (*via* route b) is virtually silica free. Similar results for mesoporous carbon made by Su *et al.,* (2005) were obtained.

4.4 CATALYST PREPARATION VIA CHEMICAL VAPOUR DEPOSITION (CVD)

Platinum (Pt) impregnation was conducted by chemical vapour deposition (CVD) method as set out in section 3.3.1. Platinum acetylacetonate [$Pt(acac)_2$)] were used in this experiment. A temperature controlled furnace was used for all experiments. Samples were prepared with a 20 % loading and were called 20% Pt/OMC.

4.4.1 X – RAY DIFFRACTION ANALYSIS OF Pt/OMC

Fig. 4.18 shows the XRD patterns for the 20 wt.% Pt loaded OMC catalysts.

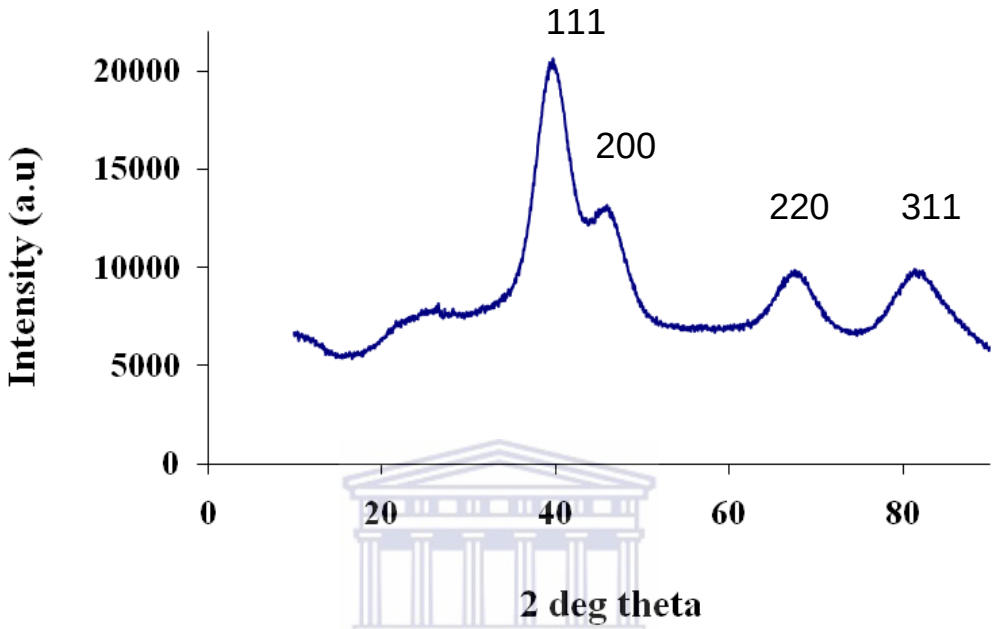

Fig 4.18: Wide angle XRD of 20 wt. % Pt/OMC catalyst

The XRD patterns for the catalyst exhibit distinct peaks at around 2θ = 39.8, 46.3, 67.5, and 81.3^{o}, which correspond to the (111), (200), (220), and (311) diffractions of the face centred cubic structure of Pt, respectively. The broadness of the peaks suggests that the Pt particle sizes in the nanometre range. The particle sizes of the 20 wt. % Pt loaded OMC were calculated from Scherrer's formula (based on Pt (111) peak) and was found to be 2.6 nm. Kong et al. (2010) found the platinum particles with a diameter of 1.5 – 2 nm in size.

4.4.2 HRTEM OF Pt/OMC (*via* route b)

Figure 4.19 shows an HRTEM image of 20 wt. % Pt supported OMC. HRTEM was performed on the Pt/OMC to assess the metal dispersion and the Pt particle size on the support. HRTEM images of Pt/OMC are presented in Figure 4.19.

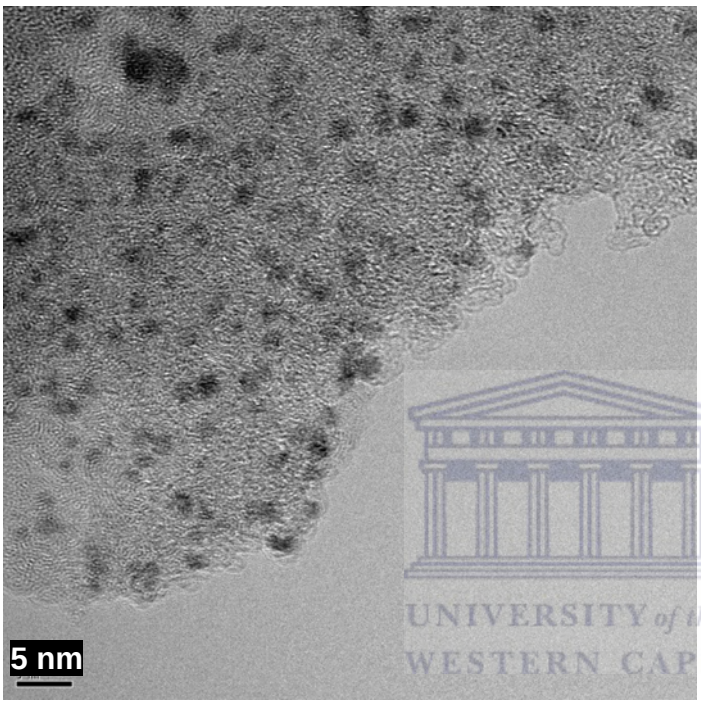

Fig. 4.19: HRTEM of the 20 wt. % Pt/OMC catalyst.

Figure 4.19 clearly show that the Pt nanoparticles are uniformly dispersed throughout the sample. The CVD method leads to Pt nanoparticles with a random distribution, which resulted in the majority of the Pt particles being present mainly on the external surfaces of mesopores rather than in the pore channels. It is very clear that that Pt has been deposited in high dispersion. The high dispersion is noted, as it illustrates the homogeneous distribution of Pt on the surface of the OMC (*via* route b) material using the CVD method. The loading of Pt was measured by energy-dispersive X-ray spectroscopy (EDS), and the average loading of Pt on the OMC was found to be 18.2% which concurred with the TGA results. (See below)

Figure 4.20 show the histogram for 20 wt. % Pt/OMC. The particle size was obtained from the average of 5 micrographs. The average of 50 particles per micrograph was used to determine the particle size.

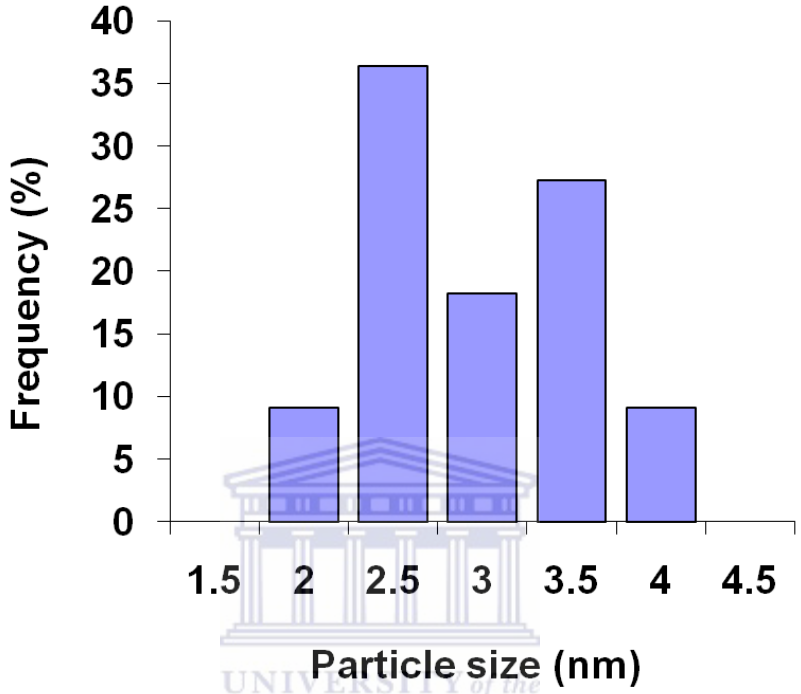

Fig. 4.20: Histogram of 20 wt. % Pt/OMC

The histogram of the 20 wt.% Pt/OMC as shown in Fig 4.20 show that the majority of Pt particle size ranges between 2.5 nm and 3.5 nm which confirms the XRD results for 20 wt. % Pt/OMC of 2.6 nm as determined by the Scherrer equation.

4.4.3 THERMOGRAVIMETRIC ANALYSIS OF 20% wt. Pt/OMC (*via* route b)

TGA was performed to determine the thermal stability of the catalyst. Figure 4.21 shows the thermogravimetric analysis (TGA) of 20 wt. % Pt/OMC performed in nitrogen using a heating rate of 10 °C min^{-1}.

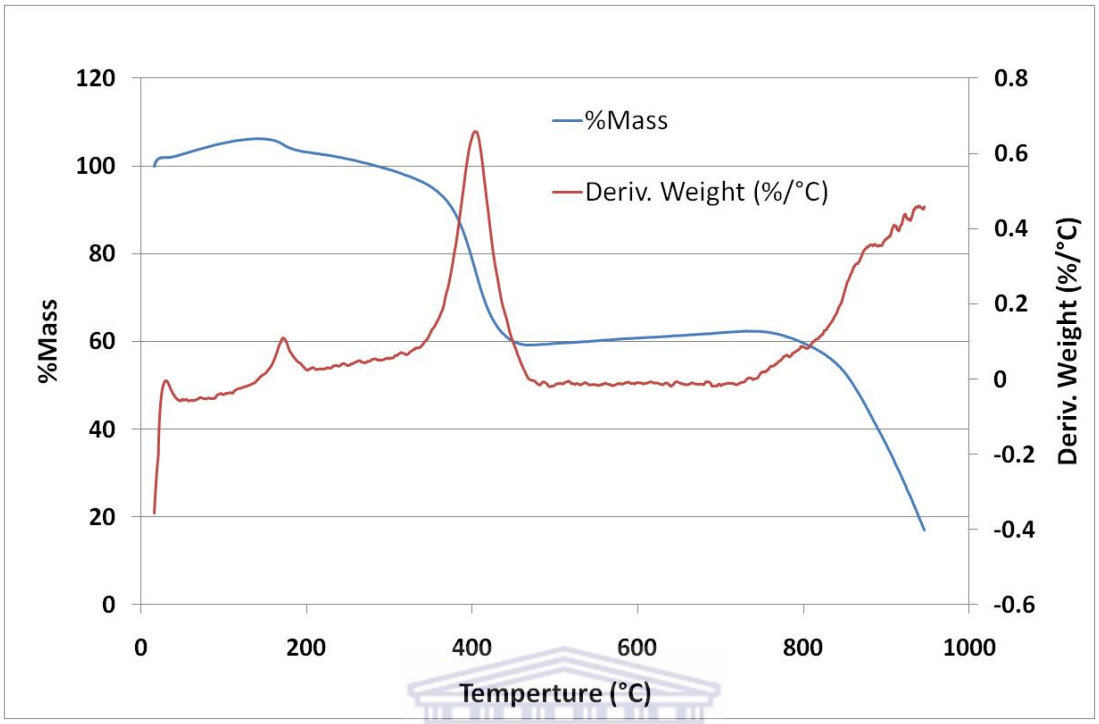

Fig. 4.21: TGA of 20 wt. % Pt/OMC

Figure 4.21 shows the thermogravimetric behaviour of 20 wt. % Pt/OMC in nitrogen. The significant weight losses related to carbon pyrolysis occurred in the temperature range of 400-500 °C that showed a 40% weight loss related to amorphous carbon and the 40% weight loss observed in the temperature range of 700-850 ^{o}C is ascribed to pyrolysis of graphitised carbon. Su *et al.,* (2005) observed a weight loss for graphitised carbon of between 550-740 ^{o}C, which is lower than that of obtained in this study. The observed residual mass of between 18-20 % at 940 ^{o}C confirms the presence of platinum (the thermogram stopped at 940^{o}C).

4.4.4 ELECTROCHEMICAL STUDIES OF Pt/OMC VS THE COMMERCIAL Pt/C JM CATALYST

The electrochemical activity of the catalysts Pt/OMC was determined by CV measurements performed in 0.5 M H_2SO_4 aqueous solution. Highly pure Ar was used prior to and during the measurements to deaerate the electrolyte. The main reason for performing CV on the prepared catalysts was to compare the activity with a commercial Pt/C JM catalyst.

In cyclic voltammetry (CV) the potential applied on the working electrode (WE) is scanned linearly from an initial value (E_i) to a second value (E_L) and then back to E_i or some other potential. The cycle can be repeated several times. The current flowing between the WE and the counter electrode (CE) is monitored throughout the study. This technique involved in changing the applied potential at a working electrode at some scan rate (both forward and reverse directions), while monitoring the current. For example, the initial scan could be in the negative direction to the switching potential and at that point the scan would be reversed and run in the positive direction. The typical response obtained from the CV is shown in Fig. 22 for the reversible redox system (Scholz, 2010).

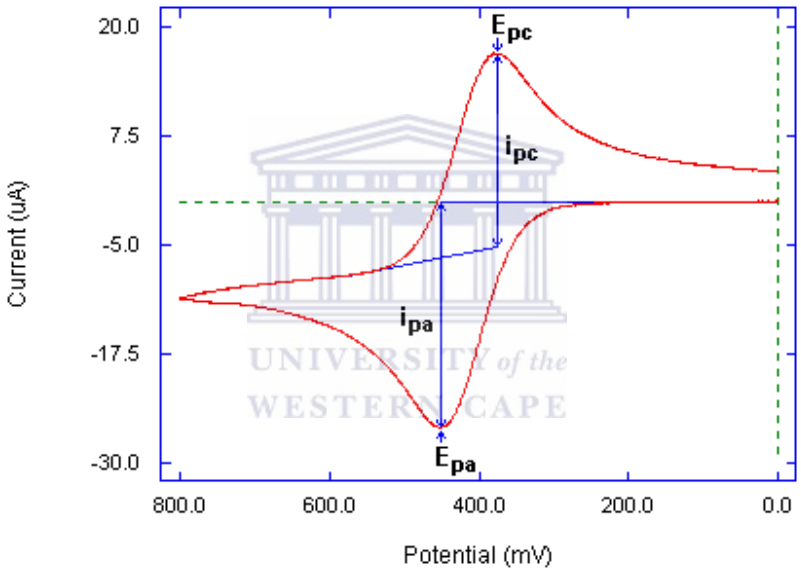

Figure 4.22: A typical cyclic voltammogram showing the important peak parameters.

In Figure 4.23, the cyclic voltammograms of the prepared catalyst and the commercial JM 40% Pt/C catalyst are compared.

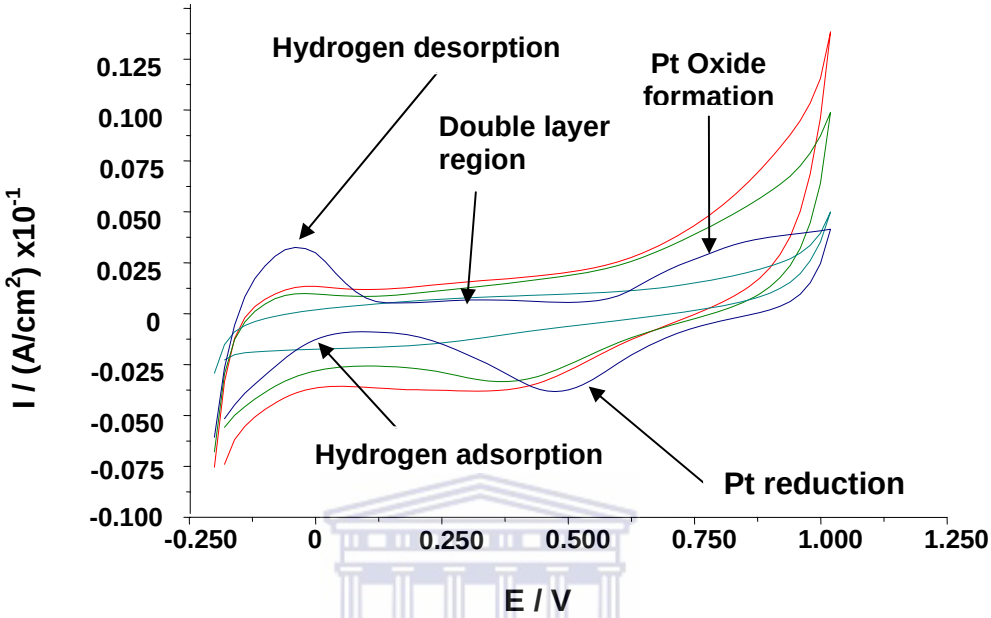

Figure 4.23: Cyclic voltammograms (CV) of 20 wt. % Pt/OMC in 0.5 M H_2SO_4 at scan rate = 50 mV/s

Blue: Pt/C (JM).
Cyan: 10% Pt/OMC
Red: 20% Pt/OMC
Green: 30% Pt/OMC

Fig.4.22 shows the cyclic voltammograms (CV) of Pt/C commercial and Pt/OMC catalysts in 0.5 M H_2SO_4. The CV obtained for the synthesized and commercial Pt/C catalyst displayed all the characteristic peaks associated with Pt/C catalysts. The peaks identified from the CV obtained are, viz., hydrogen desorption (-0.2-0.1 V), where hydrogen is desorbed from a platinum surface, the double layer region (0.15-0.56 V), Pt oxide formation (0.6-1.0 V) and platinum reduction in the regions of 0.8-0.5 V. The peak at 0.1 to –0.2 can be assigned to hydrogen adsorption onto the Pt surface as shown by Perez *et al*.,(1998).

In Figure 4.24, the methanol oxidation reaction of the prepared catalyst is shown. The main reason for doing this was to evaluate the catalyst activity for each catalyst.

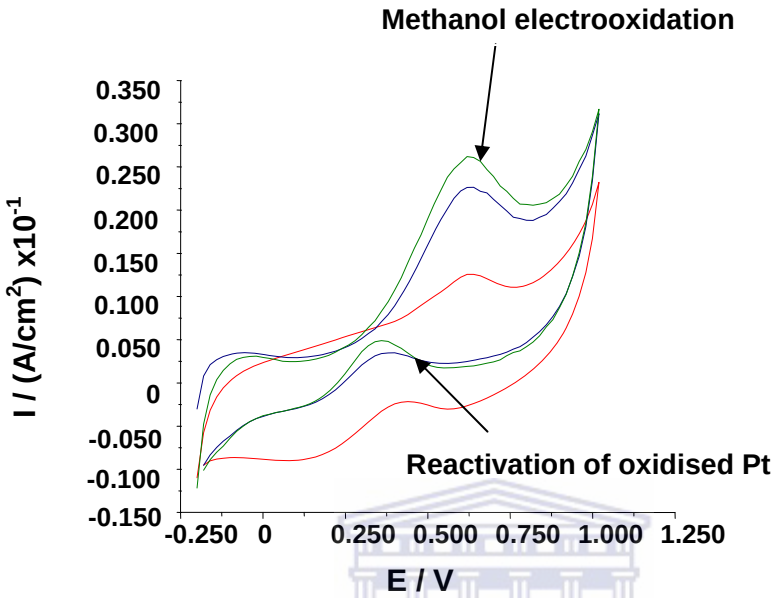

Figure 4.24: MOR (methanol oxidation reaction) of 10, 20 and 30 wt. % Pt/OMC at scan rate =50 mV/s

Red: 10% Pt/OMC
Green: 20% Pt/OMC
Blue: 30% Pt/OMC

Figure 4.24 shows the cyclic voltammograms of methanol oxidation under acidic conditions (0.5 M H_2SO_4+1.0 M CH_3OH) catalyzed by the Pt/OMC catalysts. The anodic peaks around 0.47 V in the reverse scan can be associated with the reactivation of oxidized Pt. The current peak at about 0.63 V in the forward scan is attributed to methanol electrooxidation on the Pt catalyst. It can be observed that along the direction of positive scan, the potentials of the oxidation peaks of CH_3OH for three Pt catalyst electrodes are positioned at 0.625 V. The reactions given in equations 1-4 are considered to take place in methanol solution as shown by Niu *et al.* (2008),Umeda *et al.*,(2003).

$$Pt + CH_3OH \longrightarrow Pt\text{-}CO + 4H^+ + 4e^- \quad (1)$$

$Pt + H_2O \longrightarrow Pt\text{-}OH + H^+ + e^-$ ..... (2)

$Pt\text{-}CO + Pt\text{-}OH \longrightarrow 2Pt + CO_2 + H^+ + e^-$ .....(3)

Thus, the complete electrooxidation of methanol is expressed as:

$CH_3OH + H_2O \longrightarrow CO_2 + 6H^+ + 6e^-$ .....(4)

When the potential reaches ~0.35 V in the anodic sweep, methanol molecules will adsorb the Pt with the formation of Pt-CO + $4H^+$ + $4e^-$ (Eq.(1)). The oxidation of H_2O immediately generates Pt-OH as shown in (Eq. (2)). The adsorption and oxidation will be enhanced gradually with the increased potential until the potential reaches the highest value of ~0.25 V, followed by the reaction as indicated in Eq.(3) at this potential. As the potential increases, more and more reaction products will stop the increased oxidation. This will result in the peak showing a decrease as shown in Fig.4.23. When the potential arrives at ~0.625 V in the cathodes sweep, methanol reoxidation is generated again and the peak climbs to a new high point of ~0.375 V.

Table 4.3 shows all the MOR currents obtained of the prepared catalyst. The 20%Pt/OMC catalyst showed higher currents than the other catalyst implying that this catalyst has a higher MOR activity than the other catalyst. The above results confirm that the ordered mesoporous carbon has a high application potential in DMFCs as reported by as shown by Su *et al*., (2010).

Table 4.4: MOR at 0.625V

Catalyst	**I (A/cm^2)**
10 wt. % Pt/OMC	0.125
20 wt. % Pt/OMC	0.25
30 wt. % Pt/OMC	0.225

4.5 SUMMARY OF RESULTS AND DISCUSSION

The experimental results presented in this chapter have demonstrated that mesoporous pure silica SBA-15 without loading any catalytic component can be used as a template to fabricate ordered mesoporous carbon with high surface area using sucrose as a carbon precursor to infiltrate the pores of the silica framework followed by carbonization via a pyrolytic CVD process and finally NaOH dissolution of the silica template. The CVD method affords little shrinkage of carbon framework. The experimental results for both the preparation of mesoporous silica (SBA-15) and ordered mesoporous carbon agreed with that found in literature (Piotr et al. (2005); Su *et al.* (2010)).

The most fundamental aspect of the SBA-15 Si template is that it has high surface area with uniform mesopores and this is illustrated by XRD and the BET results. The OMC material prepared using LPG (route (a)) yielded a low surface area carbon material without defined mesopores. The OMC prepared using route (b) was to a certain degree replicable since a high surface area OMC was obtained that correlated well with that reported the in literature. The resulting high surface area OMC support was obtained using SBA-15 as a sacrificial template and using sucrose as a source of carbon. This template showed that indeed a high surface area mesoporous carbon could be obtained which compared well with literature methods. Most of the silica was removed by NaOH as indicated by FTIR and EDS studies. The HRTEM images showed that the OMC microstructure was uniformly amorphous-like and showed diminishing image contrast. This may be due to the irradiation with 200 keV electrons (Smith *et al.*, (2001)).

Pt nanoparticles supported on mesoporous carbon materials have proven to be superior catalysts for various reactions and electrocatalytically active for fuel cells. This chapter presented a High Resolution TEM, thermogravimetric analysis and cyclic voltammetry study of Pt nanoparticles supported on mesoporous carbon materials. The above results showed that mesoporous carbon obtained by using sucrose (route (b)) can be used as an efficient support for the dispersion of stable Pt nanoparticles. The observed average metal nanoparticle size was 2 – 3 nm on the mesoporous carbon support. The developments of fuel cells still remain a challenging task even though there are a number of publications on the preparation of Pt nanoparticles. The CVD technique for

metal deposition on ordered mesoporous carbon assures a uniform distribution of small Pt clusters on a high specific surface area support.

CHAPTER 5

CONCLUSIONS AND RECOMMENDATIONS

5.1 CONCLUSIONS

The main objective was to synthesize ordered mesoporous carbon (OMC) materials. This involved two stages. In the first stage, a mesoporous silica template was synthesized. In the second stage, the synthesized silica samples were used to prepare the OMC support. The synthesis of an OMC required the use of sucrose to infiltrate the pores of the silica template and finally the use of NaOH for silica dissolution. The route using CVD with LPG to prepare the OMC with defined pore sizes was not successful. The sucrose pyrolysis route yielded a high surface area and mesoporous textured carbon sample. Platinum (Pt) was dispersed upon the mesoporous carbon support by means of a chemical vapour deposition method. The prepared composite carbon supported Pt catalysts were then physicochemically and electrochemically characterized. The samples were characterized by FTIR Spectroscopy, XRD, N_2 BET analysis, HRTEM, SEM, EDS, TGA, and cyclic voltammetry. The process stages were explained in detail in the experimental subsections.

The XRD diffractograms and the HRTEM micrographs indicated a high degree of mesostructural ordering in the prepared SBA-15 silica for use as a sacrificial template. The nitrogen sorption data confirmed that the SBA-15 possessed good mesostructural ordering and it was therefore an excellent choice for use as a solid template for mesoporous carbon synthesis. The carbon analogue prepared using the SBA-15 as sacrificial template with the sucrose method was found to be porous and graphitic, with a high surface area exceeding that of the parent SBA-15 silica sacrificial template and with bimodal distribution of mesopores.

The high surface area of the ordered mesoporous carbon support is required to achieve high dispersion and high loading of Pt/OMC. The total surface area of ~2100 m^2/g and pore size distribution between 2-4 nm of the OMC were similar to that reported by Li et al.(2007).

SBA-15 matrix was successfully used as a sacrificial template. The sucrose carbonization method was successfully employed in this study to produce the desired high surface area mesoporous carbon. The surface area, pore volume, and pore diameter of both SBA-15 and OMC was determined by means of N_2BET. The synthesized mesoporous carbon material was subsequently utilized as a support for the synthesis of a Pt electrocatalyst. Pt was successfully dispersed as confirmed by HRTEM and stabilized as verified by CV measurements. The synthesised Pt/OMC was compared with the commercial Pt/C JM catalyst for electrocatalytic activity and compared favourably. Different mass % loadings of Pt were loaded on the OMC using the CVD method but the 20% loaded catalyst proved to be the most active for the methanol oxidation reaction.

The addition of Pt nanoparticles on the mesoporous carbon material showed that (i) the physical structure of the mesoporous carbon was maintained, (ii) a high Pt dispersion was attained and (iii) a high Pt weight percent loading according to the XRD, HRTEM, EDS and cyclic voltammetry was accomplished.

In conclusion, an efficient approach was developed and demonstrated for the synthesis of SBA–15 using a P123 surfactant and OMC *via* a sucrose impregnation method respectively, followed by carbonization and later silica dissolution by NaOH. The surfactant-directed highly–ordered mesoporous structure was retained after the carbonization. The secondary porous structure of OMC framework was preserved after silica template dissolution with NaOH. This simple method is suitable for preparing mesoporous carbon for many potential applications, such as catalyst supports, adsorbents and hydrogen storage. The last step in this method was to impregnate Pt nanoparticles on the OMC *via a* CVD method using $Pt(acac)_2$ as a precursor.

5.2 RECOMMENDATIONS

The synthesized mesoporous carbon material was subsequently utilized as a support for the synthesis of a Pt electrocatalyst using a CVD method. It is recommended that the electrochemical study for Pt/OMC used in this study be re – examined using future characterization studies of fabricated nanophase electrocatalysts for comparison. Other catalyst preparation techniques and different loadings on the carbon support should be also investigated to further develop the method used in this study. The catalysts produced in this study can only be effectively used as good electrocatalysts after further testing to demonstrate their performance and stability in fuel cell tests.

REFERENCES

1. Ajie Henry; Alvarez Marcos M., Anz Samir J., Beck Rainer D., Diederich Franqois, Fostiropoulos K., Huffman Donald R., Kratschmer Wolfgang, Rubin Yves, Schriver Kenneth E., Sensharma Dilip, Whetten Robert L.; Characterization of the Soluble All-Carbon Molecules C_{60} and C_{70}, J. Phys. Chem. 1990, 94, 8630-8633
2. Alegre, C., Calvillo, L., Moliner, R., González-Expósito, J.A., Guillén-Villafuerte, O., Huerta, M.V.M., Pastor, E., Lázaro, M.J. Pt and PtRu electrocatalysts supported on carbon xerogels for direct methanol fuel cells. J Power Sources 2011, 196, 4226-4235.
3. Ambrosio E. P., Dumitrescu M. A., Francia C., Gerbaldi C., Spinelli P., Ordered Mesoporous Carbons as Catalyst Support for PEM Fuel Cells, FUEL CELLS 09, 2009, No. 3, 197–200
4. Ambrosio Elisa Paola, Francia Carlotta, Gerbaldi Claudio, Penazzi Nerino, Spinelli Paolo, Manzoli Maela, Ghiotti Giovanna, J, Mesoporous carbons as low temperature fuel cell platinum catalyst supports, Appl Electrochem 2008, 38, 1019–1027
5. Antolini, Ermete. Carbon supports for low-temperature fuel cell catalysts, Appl Catal B: Environ 2009, 88, 1-24.

6. Bansal R. C., Donnet J. B., Stoeckli H. F., Active Carbon, ed. Marcel Dekker, New York (1988) p9
7. Brown M. E., Introduction to Thermal Analysis Technique and Applications, Chapman and Hall (1998).
8. Chang Hyuk, Joo Sang Hoon, Pak Chanho, Synthesis and characterization of mesoporous carbon for fuel cell applications, J. Mater. Chem., 2007, 17, 3078–3088
9. Chen, Jinwei; Jiang, Chunping; Yang, Xin; Feng, Lan; Gallogly, Ethan B.; Wang, Ruilin, Studies on how to obtain the best catalytic activity of Pt/C catalyst by three reduction routes for methanol electro-oxidation, Electrochemistry Commun. 2011, 13, 314-316
10. Cherstiouk, O.V., Simonov, P.A., Savinova, E.R., Model approach to evaluate particle size effects in electrocatalysis: Preparation and properties of Pt nanoparticles supported on GC and HOPG Electrochimica Acta 2003, 48, 3851-3860
11. Coville Neil J., Tshavhungwe Alufelwi M., Mesoporous ethanesilica materials with bimodal and trimodal pore-size distributions synthesised in the presence of cobalt ions, South African J Science. 2010, 106(7/8), Art. #213, DOI: 10.4102/sajs.v106i7/8.213
12. Dandekar, A. , Baker, R.T.K. and Vannice, M.A., Carbon-Supported Copper Catalysts, J. Catalysis 1999, 184, 421–439
13. de Bruijn F. A., Marin G. B., Niemantsverdriet J. W., Visscher W. H. M., van Veen J. A. R., Characterization of Graphite-supported Platinum Catalysts by Electrochemical Methods and XPS, Surface And Interface Analysis, 1992, 19, 537-542
14. Dresselhaus M.S.; Dresselhaus S.; Saito R.; Physics of Carbon Nanotubes, Carbon, 1995, 33(7) 883-891
15. Du Y., Liu S., Ji Y., Zhang Y., Xiao N., Xiao F.-S., Ordered mesoporous silica materials (SBA-15) with good heat-resistant magnetism, J. Magnetism Magnetic Mater. 2008, 320, 1932–1936
16. Fang Yin, Gu Dong, Zou Ying, Wu Zhangxiong, Li Fuyou, Che Renchao, Deng Yonghui, Tu Bo, Zhao Dongyuan, A Low-Concentration Hydrothermal Synthesis

of Biocompatible Ordered Mesoporous Carbon Nanospheres with Tunable and Uniform Size, Angew. Chem. Int. Ed. 2010, 49, 7987 –7991

17. Fuertes B, Antonio, Nevskaia M Dasha., Control of mesoporous structure of carbons synthesized using a mesostructured silica as template, Microporous and Mesoporous Materials, 2003, 62 177–190
18. Fuertes, Antonio B., Alvarez Sonia, Graphitic mesoporous carbons synthesised through mesostructured silica templates, Carbon 2004, 42, 3049–3055
19. Gasteiger H.A., Kocha S.S., Sompalli B., Wagner F.T., Appl. Catal. B, 2005, 56, 9
20. Gaydhankar, T. R.; Samuel, V.; Joshi, P. N. Hydrothermal synthesis of MCM-41 using differently manufactured amorphous dioxosilicon sources. Mater Lett 2006, 60(7), 957-961
21. Gondongwana Z.G., M.Sc thesis UWC, Homogeneity of Nanophase Electrocatalyst supported on Mesoporous Materials, May 2006
22. Grigoriev, S.A., Mamat, M.S., Dzhus, K.A., Walker, G.S., Millet, P. Platinum and palladium nano-particles supported by graphitic nano-fibers as catalysts for PEM water electrolysis, Int J Hydrogen Energy 2011, 36, 4143-4147
23. Haines P. J., 'Thermal Methods of Analysis' Blackie Academic Professional (1995)
24. Hampsey J. Eric, Hu Qingyuan, Wu Zhiwang, Rice Lynn, Pang Jiebin, Lu Yunfeng, Templating synthesis of ordered mesoporous carbon particles, Carbon 2005, 43, 2977–2982
25. Horenstein Mark N., Electrostatics and nanoparticles: What's the same, what's different? Journal of Electrostatics 2009, 67 384–393
26. Hwang J.Y., Chatterjee A., Shen, C.H. Wang J.H., Sun C.L., Chyan Oliver, Chen C.W., Chen K.H., Chen L.C., Mesoporous active carbon dispersed with ultra-fine platinum nanoparticles and their electrochemical properties, Diamond & Related Materials 2009, 18, 303–306
27. Hyeon, T., Han, S.; Sung, Y. E.; Park, K. W.; Kim, Y. W.; High performance direct methanol fuel cell electrodes using solid-phase synthesized carbon nanocoils. Angew. Chem. 2003, 115, 4352.
28. Iijima S., Helical microtubules of graphitic carbon, Nature, 1991, 354, 56-58

29. Innocenzi Plinio and Falcaro Paolo, Order-Disorder Transitions and Evolution of Silica Structure in Self-Assembled Mesostructured Silica films Studied through FTIR spectroscopy, J. Phys. Chem. B 2003, 107, 4711 – 4717
30. Jin, Z., Wang, X., Cui, X., Synthesis and morphological investigation of ordered SBA-15-type mesoporous silica with an amphiphilic triblock copolymer template under various conditions**,** Colloids and Surfaces A: Physicochemical and Engineering Aspects 2008, 316, 27-36.
31. Joo Sang Hoon, Lee Hyung Ik, You Dae Jong, Kwon Kyungjung, Kim Jin Hoe, Choi Yeong Suk, Kang Min, Kim Ji Man, Pak Chanho, Chang Hyuk, Seung Doyoung, Ordered mesoporous carbons with controlled particle sizes as catalyst supports for direct methanol fuel cell cathodes, Carbon 2008, 46, 2034-2045
32. Katiyar Amit, Yadav Santosh, Smirniotis Panagiotis G., Pinto Neville G., Synthesis of ordered large pore SBA-15 spherical particles for adsorption of biomolecules, Journal of Chromatography A, 2006, 1122, 13–20
33. Kim T, Park S, Ryoo R. A synthetic route to ordered mesoporous carbon materials with graphitic framework. Angew Chem, Int Ed 2003, 42, 4375–9
34. Kim Tae-Wan; Chung Po-Wen; Slowing Igor I.; Tsunoda Makoto; Yeung Edward S.; Lin Victor S.-Y., Structurally Ordered Mesoporous Carbon Nanoparticles as Transmembrane Delivery Vehicle in Human Cancer Cells, Nano Lett., 2008, 8, 11
35. Kokunešoski, M., Gulicovski, J., Matović, B., Logar, M., Milonjić, S.K., Babić, B. Synthesis and surface characterization of ordered mesoporous silica SBA-15, Materials Chemistry and Physics 2010, 124, 1248-1252
36. Kong Ling-Bin, Li Heng, Zhang Jing, Luo Yong-Chun and Kang Long, Platinum catalyst on ordered mesoporous carbon with controlled morphology for methanol electrochemical oxidation, Applied Surface Science 2010, 256, 6688–6693
37. Kresge C.T., Leonowicz M.E., Roth W.J., Vartuli J.C., Beck J.S., Ordered mesoporous molecular sieves synthesized by a liquid-crystal template mechanism**,** Nature 1992, 359, 710
38. Kroto H. W, Heath J. R, O'Brien S. C, Curl R. F, Smalley R. E, C60: Buckminsterfullerene *Nature* 1985, 318, 162–3
39. Kratschmer, W., FotiropouLan, K., Huffmon, D.R., Chem. Phys.1990, 170, 167

40. Kruk, M., Kohlhaas, K.M., Dufour, B., Celer, E.B., Jaroniec, M.,Matyjaszewski, K., Ruoff, R.S., Kowalewski, T.: Microporous Mesoporous Mater. 2007,102, 178–187

41. Kumar Mukul and Ando Yoshinori, Chemical Vapour Deposition of Carbon Nanotubes: A Review on Growth Mechanism and Mass Production, J. Nanosci. Nanotechnol. 2010, 10, 6

42. Langley P. J., Hulliger J., Nanoporous and mesoporous organic structures: new openings for materials research, Chem. Soc. Rev., 1999, 28, 279–291

43. Li Hui-Qiao, Liu Rui-Li, Zhao Dong-Yuan, Xia Yong-Yao; Electrochemical properties of an ordered mesoporous carbon prepared by direct tri-constituent co-assembly; Carbon 2007, 45, 2628–2635

44. Lin, C. F.; Zhang, X.; Lin, H.; Wang, N.; Li, J. B.; Yang, X. Z, Synthesis of ordered mesoporous carbon using MCM-41 mesoporous silica as template, Adv Mater Res 2006, 11-12 , 543-546

45. Mhlanga S.D.; Mondal K.C.; Naidoo N.; Kunjuzwa N.; Witcomb M.J.; N.J. Coville; Synthesis and study of carbon microspheres for use as catalyst support for cobalt; South African Journal of Science 2009, 105, July/August.

46. Moreno-Castilla Carlos, Carrasco-Mar´ın Francisco, Lo´pez-Ramo´n M. Victoria, Alvarez-Merino Miguel A., Chemical and physical activation of olive-mill waste water to produce activated carbons, Carbon 2001, 39, 1415–1420

47. Morishige, K., Uematsu, H., Tateishi, N. Comparative study of liquid-solid phase transition of nitrogen in controlled pore glass and SBA-15: Accurate pore size of conventional mesoporous materials, Journal of Physical Chemistry B 2004, 108 7241-7246

48. Niu J.J., Wang J.N., Electrochim. Acta 2008, 53, 8058

49. Okada Kiyoshi, Yamamoto Nobuo, Kameshima Yoshikazu, Yasumori Atsuo, Porous properties of activated carbons from waste newspaper prepared by chemical and physical activation, Journal of Colloid and Interface Science 2003, 262, 179–193

50. Orge, C. A.; Sousa, J. P. S.; Goncalves, F.; Freire, C.; Orfao, J. J. M.; Pereira, M. F. R. Development of Novel Mesoporous Carbon Materials for the Catalytic Ozonation of Organic Pollutants Catal Lett 2009, 132, 1-9

51. Osswald J, Fehr K. T, FTIR spectroscopic study on liquid silica solutions and nanoscale particle size determination, J Mater Sci 2006, 41, 1335–1339

52. Perathoner S., , Gangeri M., Lanzafame P., Centi G., Nanostructured Electrocatalytic Pt–Carbon Materials for Fuel Cells and CO Conversion, Kinetics and Catalysis, 2007, 48(6) 877–883

53. Perez Joelma, Gonzalez E.R. , Ticianelli E.A., Electrochimica Acta 1998, 44, 1329-1339

54. Petrik L.F. ; Godongwana Z.G.; Iwuoha E.I.; Platinum nanophase electro catalysts and composite electrodes for hydrogen production; Journal of Power Sources 2008, 185, 838–845

55. Piotr Kuśtrowski, Lucjan Chmielarz, Roman Dziembaj, Pegie Cool, Vansant Etienne F., Modification of MCM-48-, SBA-15-, MCF-, and MSU-type Mesoporous Silicas with Transition Metal Oxides Using the Molecular Designed Dispersion Method, J. Phys. Chem. B, 2005, 109 (23) 11552–11558

56. Pozio, A., De Francesco M., Cemmi A., Cardellini F., Giorgi L., Comparison of high surface Pt/C catalysts by cyclic voltammetry, J. Power Sources 2002, 105 13–19

57. Rios Rachel RibeiroVieira Azzi; Alves Dênio Eduardo; Dalmázio Ilza; Bento Sílvio Fernando Vargas; Donnici Claudio Luis; Lago Rochel Monteiro, Tailoring Activated Carbon by Surface Chemical Modification with O, S, and N Containing Molecules, Materials Research, 2003, 6(2) 129 – 135

58. Rodriguez-Reinoso F., The role of carbon materials in heterogeneous catalysis Carbon, 1998, 36, 159-175

59. Ryoo R.; Joo S. H.; Jun S.; Synthesis of Highly Ordered Carbon Molecular Sieves via Template-Mediated Structural Transformation, J. Phys. Chem. B, 1999, 103, 37

60. Ryoo Ryong, Joo Sang Hoon, Jun Shinae, Synthesis of Highly Ordered Carbon Molecular Sieves via Template-Mediated Structural Transformation, *J. Phys. Chem. B*, 1999, 103 (37), 7743–7746

61. Ryoo, R.; Joo, S. H.; Jun, S.; Tsubakiyama, T.; Tearasaki, O. Stud. Surf. Sci. Catal. 2001, 135, 07-O-01

62. Sakintuna Billur, Yurum Yuda, Templated Porous Carbons: A Review Article, Ind. Eng. Chem. Res. 2005, 44, 2893-2902
63. Sang, Lung-Ching; Vinu, Ajayan; Coppens, Marc-Olivier Ordered mesoporous carbon with tunable, unusually large pore size and well-controlled particle morphology J Mater Chem 2011, 21(20), 7410-7417
64. Scholz, Fritz, Electroanalytical Methods: Guide to Experiments and Applications 2nd Ed, 2010 Springer
65. Setoguchi, Yukako M.; Teraoka, Yasutake; Moriguchi, Isamu; Kagawa, Shuichi; Tomonaga, Nariyuki; Yasutake, Akinori; Izumi, Jun. Rapid room temperature synthesis of hexagonal mesoporous silica using inorganic silicate sources and cationic surfactants under highly acidic conditions. Journal of Porous Mater 1997, 4, 129-134.
66. Shimura F., in semiconductor silicon crystal technology, Academic Press Inc, San Diego (1989)
67. Smith B.W., Luzzi D.E., Electron irradiation effects in single wall carbon nanotubes, Journal of Applied Physics 2001, 90, 3509
68. Steigerwalt. E.S, Deluga. G.A, Cliffel. D.E. Lukehart. C.M. J. Physical Chemistry, 2001, 105, 8097-8101.
69. Stiles A. B., Catalyst Supports and Supported Catalysts, Theoretical and Applied Concept, Butterworths, Boston (1987)
70. Stoeckli H. F., Microporous carbons and their characterization: The present state of the art Carbon, 1990, 28, 1-6
71. Su Fabing, Poh Chee Kok, Tian Zhiqun, Xu Guangwen, Koh Guangyong, Wang Zhan, Liu Zhaolin, Lin Jianyi, Electrochemical Behavior of Pt Nanoparticles Supported on Meso- and Microporous Carbons for Fuel Cells, Energy Fuels, 2010, 24, 3727-3752
72. Su Fabing, Zeng Jianhuang, Bao Xiaoying, Yu Yaoshan, Lee Jim Yang, Zhao X. S., Preparation and Characterization of Highly Ordered Graphitic Mesoporous Carbon as a Pt Catalyst Support for Direct Methanol Fuel Cells, Chem. Mater. 2005, 17, 3960-3967

73. Su Fabing, Zeng Jianhuang, Yu Yaoshan, Lv Lu, Lee Jim Yang, Zhao X.S., Template synthesis of microporous carbon for direct methanol fuel cell application, Carbon 2005, 43, 2366–2373

74. Suttisawat Y., Rangsunvigit P., Kitiyanan B., Williams M., Ndungu P., Lototskyy M.V., Nechaev A., Linkov V., Kulprathipanja S., Investigation of hydrogen storage capacity of multi-walled carbon nanotubes deposited with Pd or V, International Journal of Hydrogen Energy 2009, 34, 6669-6675

75. Taguchi Akira, Schuth Ferdi, Ordered mesoporous materials in catalysis, Microporous and Mesoporous Materials 2005, 77, 1 – 45

76. Tamai H., Shiraki K., Shiono T., Yasuda H., Surface functionalization of mesoporous and microporous activated carbons by immobilization of diamine J. Coll. Int. Sci., 2006, 295, 299-302

77. Taniguchi N., "On the Basic Concept of 'Nano-Technology'," Proc. Intl. Conf. Prod. Eng. Tokyo, Part II, Japan Society of Precision Engineering, 1974.

78. Thurier Cyril, Doppelt Pascal , Platinum OMCVD processes and precursor chemistry, Coordination Chemistry Reviews 2008, 252, 155–169

79. Tusi, M.M., de Oliveira Polanco, N.S., Brandalise, M., Correa, O.V., Villalba, J.C., Anaissi, F.J., Neto, A.O., Spinacé, E., PtRu/Carbon hybrids with different Pt:Ru atomic ratios prepared by hydrothermal carbonization for methanol electro-oxidation. Int J Electrochem Sci 2011, 6, 484-491

80. Twigg Martyn V.,“Carbons and Carbon Supported Catalysts in Hydroprocessing”, Platinum Metals Rev., 2009, 53(3), 135–137

81. Umeda M., Kokubo M., Mohamedi M., Uchida I., Electrochim. Acta 2003, 48 1367

82. Van Tendeloo G, Lebedev O I , Collart, Cool O.P, Vansant E.F, Structure of nanoscale mesoporous silica spheres, , J. Phys.: Condens. Matter 2003, 15 S3037–S3046

83. Vartuli, J. C.; Kresge, C. T.; Leonowicz, M. E.; Chu, A. S.; McCullen, S. B.; Johnson, I. D.; Sheppard, E. W. Synthesis of mesoporous materials: liquid-crystal templating versus intercalation of layered silicates, Chem Mater 1994, 6, 2070-7

84. Vinu Ajayan, Mori Toshiyuki, Ariga Katsuhiko, New families of mesoporous materials, Science and Technology of Advanced Materials 2006, 7, 753–771

85. Wang Lingzhi; Wang Lei; Zhang Jinlong, Direct synthesis of Cr-MCM-48-like large pore mesoporous silica, J Mater Sci 2009, 44, 6512–6518

86. Webb. P.A, Orr. C, Camp. R.W, Olivier. J.P, Yunes. Y.S. Analytical Methods in Fine Particle Technology, Georgia, Micromeritics Instrument Corporation, 1997 1: 11 – 14, 6: 219 - 268

87. Yang, H.; Yan, Liu, Y.; Zhang, F.; Zhang, R.; YanMeng, Y.; Li, M.; Xie, S. ; Tu, B.; Zhao, D., A Simple Melt Impregnation Method to Synthesize Ordered Mesoporous Carbon and Carbon Nanofiber Bundles with Graphitized Structure from Pitches, J. Phys. Chem. B 2004, 108, 17320–17328

88. Zeng, J. , Su, F. , Han, Y.-F., Tian, Z. , Poh, C.K. , Liu, Z. , Lin, J. , Lee, J.Y., Zhao, X.S. Pt nanoparticles supported on sandwiched Ru/carbon nanocomposite as a bimetallic catalyst for methanol electrooxidation, J Phys Chem C, 2008, 112 15908-15914

89. Zhao D, Feng J, Huo Q, Melosh N, Fredrickson GH, Chmelka BF, et al. Triblock copolymer syntheses of mesoporous silica with periodic 50 to 300 Angstrom pores. Science, 1998, 279, 548–52

90. Zhao Dongyuan, Feng Jianglin, Huo Qisheng, Melosh Nicholas, Fredrickson Glenn H., Chmelka Bradley F., Stucky Galen D. , Triblock Copolymer Syntheses of Mesoporous Silica with Periodic 50 to 300 Angstrom Pores, Science , 1998, 279, 548-552

91. Zhao W.; Li Q.; Synthesis of nanosize MCM-48 with high thermal stability, Chem. Mater., 2003, 15, 4160

92. Zhao X. S., Su Fabing, Yan Qingfeng, Guo Wanping, Bao Xiao Ying, Lv Lu, Zhou Zuocheng, Templating methods for preparation of porous structures, J. Mater. Chem., 2006, 16, 637–648

93. Zhu, Zhen; Jiang, Hua; Susi, Toma; Nasibulin, Albert G.; Kauppinen, Esko I. The Use of NH3 to Promote the Production of Large-Diameter Single-Walled Carbon Nanotubes with a Narrow (n,m) Distribution, J. Am. Chem. Soc. 2011, 133(5), 1224-1227